BEHAVIOR OF SOLID WALL AND SANDWICH FIBER REINFORCED POLYMER LINERS USED FOR REHABILITATION OF BURIED PIPES

by

Anita Shiny Kanagaraj

Submitted in partial fulfilment of the requirements
for the degree of Master of Applied Science

at

Dalhousie University
Halifax, Nova Scotia
April 2020

© Copyright by Anita Shiny Kanagaraj, 2020

To my beloved parents and elder sister who have always been there to support and encourage me. To God Almighty for all his mercies.

This thesis is dedicated to you.

TABLE OF CONTENTS

LIST OF TABLES

LIST OF FIGURES

ABSTRACT

This research was focused on studying the behavior of fiber reinforced polymer (FRP) liners that could be bonded inside deteriorated buried pipes, as an effective rehabilitation system to increase strength and stiffness. The results of thin solid wall and sandwich FRP liners subjected to transverse compressive loading are discussed in this thesis. Specimens were tested under parallel plate loading method according to ASTM D2412–11 standards, using a customized compression testing machine with string potentiometers to measure the diametrical deflections. Solid wall glass fiber reinforced polymer (GFRP) and carbon fiber reinforced polymer (CFRP) liners, sandwich liners with GFRP/CFRP facesheets and three-dimensional (3D) woven fabric core, and sandwich liners with GFRP/CFRP facesheets and bulkermat core, were tested to find the diametrical deflection, pipe stiffness (PS) and stiffness factor (SF) at 1%, 2.5%, 5% and 10% vertical diametrical deflection. The structural behavior and mechanical properties of the FRP liners were used to develop an analytical model to determine the diametrical ring deflection occurring in the vertical and horizontal directions that causes geometric non-linearity while deforming substantially and corresponding strains at springline and crown/invert positions. The model was in good agreement with the experimental data and was able to predict the failure mode of specimens with linear elastic material behavior that was fully composite until failure in transverse compression. A parametric study was also conducted to analyze the effect of liner diameter, core thickness, facesheet thickness and shape geometry on liner behavior to establish a data platform for design purposes. Overall, the strength and ring stiffness based on vertical diametrical deflections were determined to understand the behavior and mechanical performance of thin solid wall and sandwich liners under transverse compression.

LIST OF ABBREVIATIONS AND SYMBOLS USED

ABBREVIATIONS

ASTM	American Society for Testing and Materials
AWWA	American Water Works Association
B	Bulkermat Core
CFRP	Carbon Fiber Reinforced Polymer
CIPP	Cured-In-Place Pipe
DAQ	Data Acquisition System
FDA	Finite Difference Analysis
FEA	Finite Element Analysis
FRP	Fiber Reinforced Polymer
GFRP	Glass Fiber Reinforced Polymer
HDD	Horizontal Directional Drilling
HDPE	High Density Polyethylene
NEB	National Energy Board
PCCP	Prestressed Concrete Cylinder Pipe
PI	Popularity Index
PS	Pipe Stiffness
PVC	Poly-Vinyl Chloride
RCP	Reinforced Concrete Pipes
RPMP	Reinforced Polymer Mortar Pipe
SF	Stiffness Factor
SG	Strain Gauges
SP	Sandwich Pipes
UTM	Universal Testing Machine
W	3-D Woven Fabric Core

SYMBOLS USED

a	Horizontal Radius of Elliptical Ring
b	Vertical Radius of Elliptical Ring
c	Core Thickness
d	Internal Diameter of the Pipe
D_L	Deflection lag factor
E	Elastic Modulus
EI	Flexural Rigidity or Stiffness Factor
F	Load Applied
G	Shear Modulus
I	Moment of Inertia
M	Moment
N	Longitudinal Force
n	Number of Layers
NA	Neutral Axis
Q	Horizontal Force
r	Mean Radius
R	Ring Radius
t	Thickness of the Pipe
t_f	Facesheet Thickness
U	Strain Energy
V	Shear Force
W_C	Vertical soil load on the pipe
W_L	Live load on the pipe
Δx	Displacement in the Horizontal Direction
Δy	Displacement in the Vertical Direction
ρ	Radius of Curvature

ACKNOWLEDGEMENTS

I would like to extend my sincere gratitude to Dr. Pedram Sadeghian who has been my mentor and supervisor. I am thankful for his support, guidance, motivation and patience throughout my program. I would like to thank my committee members, Dr. Navid Bahrani and Dr. Fadi Oudah for taking the time to review the manuscript and providing me with constructive feedback.

The support and assistance provided by Mr. Jordan Maerz, Mr. Jesse Keane and Mr. Brian Kennedy in the lab while fabricating and testing specimens is greatly appreciated. I would like to acknowledge QuakeWrap Inc. (Tucson, AZ, USA) for providing all the materials that was used for this research.

I thank my family, friends, colleagues and well-wishers for their continuous love and encouragement. Above all, I thank God for making this thesis possible.

CHAPTER 1 INTRODUCTION

1.1 MOTIVATION

Canada's buried infrastructure like culverts, stormwater drains, sewers, water conduits, shielding pipes and tunnels have been in service since early 1940's, majority of which are in the end of design service life. As of 2019, there are over 49,000 units of culverts across the country, of which 40% are in fair to worse condition. There are 339,000 kilometers of local and transmission potable water pipelines of which 25% are in poor state and of the 267,000 kilometers of sewer lines, 20 – 25% require rehabilitation. The stormwater infrastructure tallies to 304,000 kilometers, of which 40% stormwater culverts and pipelines are in less known utility conditions and are likely to be restored or rehabilitated (CIRC 2019). According to Canadian Infrastructure Report Card 2019, the condition profile of these structures has worsened significantly since 2016. With the numbers increasing rapidly, it is critical to find efficient, sustainable and economic solutions to improve the existing state of buried infrastructure.

Throughout this thesis, the term "pipes" is referred to both pipes and culverts. Buried pipes are often made from concrete or corrugated steel, which deteriorate while aging. Long time exposure to various physical and chemical parameters like soil pressure, internal pressure of conveyed material, chemical attacks, freeze and thaw action, corrosion etc. reduces the strength, durability and service life of the structure. A deteriorated pipe causes disruption to the traffic, widespread pollution, local flooding, emission of harmful gasses etc. Various trenchless rehabilitation techniques such as sliplining, cured-in-place pipe (CIPP) lining, pipe jacking, fold and reformed piping, pipe bursting, spot repair etc. have been used to reline, repair and improve the life of such deteriorated pipes. Popularity Index (PI) is used

to assess the popularity of pipe rehabilitation and repair methods based on frequency of the responses and total number of responses for each type of trenchless technology. Techniques like sliplining has a PI of 93.2% and CIPP lining has a PI of 75% in the United States and can be used to rehabilitate both small and large diameter pipes (Syachrani et al. 2010; Simpson et al. 2017; Zhao et al. 2002). However, it is difficult to rehabilitate pipes with bents using sliplining or CIPP, as it requires extensive preparation work on the existing deteriorated pipe. In such cases, hand lay-up technique is an accessible solution to rehabilitate pipes where direct human interference is possible (Abraham and Gillani 1999; Walsh 2017). Especially, in case of large diameter prestressed concrete pipes, rehabilitation requires substantial excavation and pre-stabilization of the pipe section which is time consuming and expensive. Also, post-tensioning the entire system after rehabilitation is laborious and hence strengthening using fiber reinforced polymer (FRP) liners has proven to be a viable solution (Lee and Karbhari 2005). Hand lay-up method of lining is effective to rehabilitate deteriorated pipes with diameters over 2 m, for which the liner material is bonded to the interior of the pipe. FRP composites are preferred for this purpose because of their high strength-to-weight ratio/ specific strength, dimensional stability, anti-corrosion, low maintenance cost, durability over a range of imposed conditions and good mechanical properties (Rafiee R. 2016; Park et al. 2014; Rafiee and Habibagahi 2018). The FRP liners act as, a reinforcing material to supplement the inadequate steel in the original pipeline, an impervious layer to stop leakage and a protection layer to control corrosion. The prominent aspect of using an FRP liner is the smoothness it provides inside the pipe section. Smoothness translates to less friction and hence resists scale deposits, thereby improving the pipe flow with a minimal or no reduction in flow capacity across the pipe.

Solid wall FRP liners can be used to rehabilitate deteriorated concrete and steel pipes with a minimal decrease in flow capacity and increased pressure rating. This could be achieved by bonding either unidirectional or bidirectional fabrics inside the pipe. Based on design requirements, one or more layers of the fabric can be applied to obtain the required strength and stiffness in the desired direction. Fabric strips are applied in the hoop direction such that the length of the strips are equal to circumference of the pipe. An end overlap is provided to help develop forces in the fiber. The longitudinal ends of the fabric are butt jointed with the adjacent fabric, along the length of the pipe to ensure the development of full strength of fibers in that direction. The overlaps in hoop direction are to be positioned along flow direction, to act as shingles which safeguards the fabric against water under high pressure entering behind it and debonding the liner from pipeline. Bidirectional fabrics can be manufactured with different amounts of fibers oriented in both longitudinal and lateral directions (Karbhari 2015; Aylor and Hirtz 1990). In both cases, care must be taken to properly fit and align the fibers to achieve the required structural capacity. Based on various tests it is evident that the compressive strength of FRP's are usually lower than their tensile strength. Also, thin FRP sheets have proven to have less stiffness. (Das and Baishya 2016; Wang et al. 2016; Wakayama et al. 2002; Deniz et al. 2013; Tarakcioglu et al. 2007; Rafiee and Elasmi 2017; Lee and Karbhari 2005; Rafiee and Habibagahi 2018; Houssam and Sean 2001). This leads to the use of multiple layers of FRP's during design to gain sufficient moment of inertia, to attain the required stiffness. Using multiple layers increases the cost and extends the duration of rehabilitation work. To overcome these shortcomings, sandwich liners can be used to achieve adequate thickness and stiffness, as that of a solid wall liner, which is also beneficial in terms of cost and structural stability.

Sandwich composites have found a profound role, in the field of repair and rehabilitation to improve the efficiency and longevity of deteriorated structures, while sufficiently optimizing the overall density after bonding. Sandwich liners have very thin but tough facesheets and a thick, lightweight and low density core. The flexural strength increases as the core separates the two facesheets by increasing the distance between them to produce an increased moment of inertia (McCracken and Sadeghian 2018; Betts et al. 2018; Allen 2013). Though sandwich composites are of lightweight and have low density, they provide high strength and stiffness to the bonded structure. Compressive and tensile stresses due to bending are resisted by the FRP facesheet, while shear stresses are resisted by the core material. The bending stiffness and strength of such structurally aligned sandwich composites are much larger than that of a single solid plate of the same total weight made of the same materials as that of facesheets, which makes them preferable for high performance structural rehabilitation (Zinno et al. 2010). Also, since sandwich liners can be custom made with flexible skin and core rolls, they are able to fit to any shape and size of the cross section of deteriorated pipe.

1.2 RESEARCH OBJECTIVES

This research was focused on:

- Understanding the actual behavior and structural capabilities of solid wall and sandwich FRP liners under transverse compression.
- Developing an analytical model to find deflections and strains by considering the geometric non-linear behavior of liners as they largely deformed under loading.
- Establishing a data platform to develop a reliable design methodology for the rehabilitation of buried infrastructure using FRP liners.

1.3 RESEARCH SCOPE

For this study, thin FRP solid wall and sandwich liners were fabricated and tested under transverse compression. Mechanical properties and structural behavior were studied and the pipe stiffness (PS) and stiffness factor (SF) according to ASTM D2412-11 (2018) standards were predicted. An analytical model was developed using an iterative procedure to find the large deformations that occurred due to loading and thus creating the geometric non-linearity in solid wall and sandwich liners. A simple model to predict the PS and SF of liners was also developed. This study has used material properties from a previous work on partial-composite behavior of sandwich beams composed of fiberglass facesheets and woven fabric core (McCracken and Sadeghian 2018).

1.4 THESIS LAYOUT

This thesis is structured with five chapters. Chapter 1 discusses the motivation for the study, research objectives and scope. Chapter 2 investigates the literature for various rehabilitation techniques to strengthen deteriorated pipes. Studies on ring deflection, PS, SF and other analytical and numerical modelling will also be reviewed. Chapter 3 details the experimental program and reviews the test matrix, material properties, specimen fabrication, test setup and instrumentation. The experimental results will be provided and discussed. Chapter 4 includes the detailed description of the analytical model and its verification against the test data. A parametric study discussing the effects of four parameters on pipe behavior is also be presented. Chapter 5 provides a brief conclusion and recommendation for future research developments focused in the field of rehabilitation of buried infrastructure.

CHAPTER 2 LITERATURE REVIEW

2.1 BACKGROUND

Buried infrastructures are required to withstand loads generated by fill cover, road traffic and internal pressure of the gas or fluid. Currently, over hundreds of thousands of pipes served under highways and the NEB (National Energy Board) of Canada are 50 years or older. In a survey conducted by Bhattachar (2007) requesting information from departments of transportation in the US and Canada, 13% of the participants indicated that their culverts were at the limit of their service life. When structures approach or reach their design service life, agencies have three options: repair, rehabilitate or replace (Ballinger and Drake 1995; Garcíaa and Moore 2015; Wyant 2002). It is nearly impossible to replace every deteriorated pipe due to lack of government funding and the high traffic disruption it causes, leaving rehabilitation as an alternative (Mai et al. 2014).

Substantial reconstruction programs are now conducted for buried structures built during the early infrastructural booms in the US and Canada. Circular reinforced concrete pipes (RCP) were the commonly used structure as highway culverts and sewers for over a century. Now, they necessitate prohibitively expensive infrastructure replacement, or alternatively rehabilitation. Having rehabilitated some of these concrete culverts with a less economic impact on transportation network disruption and user delays, the pipes are now able to carry higher surface loads than those they were originally designed for (Simpson et al. 2017).

No-dig or less dig trenchless technology is a start-of-the-art system used to rehabilitate buried infrastructure. Commonly used techniques include Relining, Cured-In-Place Pipe (CIPP), Micro tunneling, Tunneling, Horizontal Directional Drilling (HDD), Sliplining,

Fold-and-Reformed pipe, Pipe Jacking, Pipe Bursting, Spot Repair, Spiral Wound, and Shotcreting. It is important that engineers keep abreast of all the existing and emerging trenchless technologies, and also the associated cost in order to make appropriate decisions on budgeting, rehabilitation priorities and scheduling (Zhao et al. 2002). According to the report released by Zhao et al. (2002), the costliest method was micro tunneling which was valued at USD 9.52/mm/m, followed by pipe jacking at USD 4.29/mm/m as shown in Table 2-1. These two methods were much expensive than the open cut method which was at USD 3.85/mm/m. The cheapest method was relining the pipe at USD 0.95/mm/m. It is critical to understand that although relining is the least expensive method to practice, the total cost incurred for a project is also majorly reliant on the cost of latest or contemporary materials available and skilled labor charges.

Table 2- 1 Average Cost of Trenchless Techniques (Zhao et al. 2002)

Method	Overall average cost† ($*/mm dia./m length)	Diameter range‡, mm				# of data records from T.T. Magazine
		Small (≤300)	Medium (330 – 940)	Large (960 –1,830)	Very large (> 1,830)	
		($/m)	($/m)	($/m)	($/m)	
Microtunneling	9.52	2,614	4,770	15,399	46,898	51
Tunneling	3.74	-	1,962	7,093	7,969	24
CIPP	1.38	299	531	2,654	-	39
HDD	2.97	265	1,791	6,239	-	10
Sliplining	1.38	231	988	2,441	2,567	16
Pipe Bursting	2.20	726	1,165	-	-	11
Pipe Jacking	4.29	-	-	7,540	9,515	6
Relining	0.95	295	-	-	-	6
Open Cut	3.85	609	2,314	2,225	-	14

† - For the reported projects that contained more than one diameter, the average diameter was used for determining the overall average cost.

‡ - The data records that could not be separated for the diameter ranges were not used in these diameter ranges, but used in the overall average.

* - All costs are expressed as the 2001 value and in $ CDN. $US 1 = $1.48 CDN.

This research was focused on using FRP composites to repair and strengthen deteriorated buried pipes. This could be achieved by bonding a structural FRP liner inside a pipe by means of sliplining or wet-layup techniques. For pipes with larger diameters, wet lay-up technique is preferred, where skilled laborers work from within the pipe to bond the liner against the pipe wall like a wallpaper. For smaller diameter pipes, packers could be used to deliver the materials to the point requiring strengthening (Ehsani 2019).

2.2 Behavior & Analysis of FRP Pipes in Transverse Compression

2.2.1 Introduction

While a substantial record is made available in the literature on the structural behavior of FRP pipes, research conducted specifically on using FRP composites as pipe liners is minimal. In the limited studies available, Ehsani (2019) had assumed that the host pipe will eventually disintegrate completely and the liner by itself will have to act as a new pipe. Though it poses an extremely conservative view, the deteriorated host pipe essentially requires it so that the new system is able to resist all internal and external loads independently of the former. The fundamental behavioral characteristics of FRP liners are similar to FRP pipes of the same nature. Hence, this section will review the general behavior and analysis of FRP pipes which are subjected to transverse compression.

The study of behavior of pipes without the presence of soil is an important method of examining its performance, setting limit states and testing the pipe for quality control. To check the stability and serviceability of FRP pipes under a maximum deflection, parallel plate load test is highly preferred. In this test, a sample specimen is compressed with a load (F) under a loading plate to simulate the buried conditions. The pipe behavior and the shape that the pipe will take during its service life is studied. As the pipe deflects into an oval or

elliptical shape, stresses and strains are generated in the pipe wall (Corey 2015).

Typically, this test is used to find the PS and load – deflection characteristics of pipe which are useful in design. The PS is determined from the results of the test and is given as the force (F) per unit deflection (Δy) per unit length of pipe. It is given in units of kPa (or psi) generally (ASTM 2018).

$$PS = {}^{F}/_{\Delta y} \tag{2-1}$$

Spangler (1941) also derived a PS equation for thin elastic rings based on the Castigliano's Theorem as presented in Equation 2-2. For smaller pipe deflections, the equation was in good agreement with the experimental results. For deflections greater than 5% of the vertical diameter, a small divergence of the plotted experimental PS from the equation presented was observed.

$$PS = {}^{EI}/_{0.149\, r^3} \tag{2-2}$$

where E is the elastic modulus, I is the moment of inertia, and r is the mean radius of pipe.

2.2.2 Solid Wall Pipes under Transverse Compression

Park et al. (2014) studied and compared the pipe stiffness of three GFRP pipes obtained from experimental testing under parallel plate loading, theoretical analysis and a Finite Element Analysis (FEA). GFRP pipes with a length and diameter of 300 mm and a thickness of 9 mm were used for this study. The specimens had an average tensile strength of 113.05 MPa and an elastic modulus of 21.4 GPa. The load at 5% ring deflection was found to be 10.78kN and the PS was recorded as 718.4 kN/m^2 based on experimental testing. Park et al. (2014) also discussed a theoretical solution to find the PS based on both the vertical and horizontal deflections using the elastic curved bar theory.

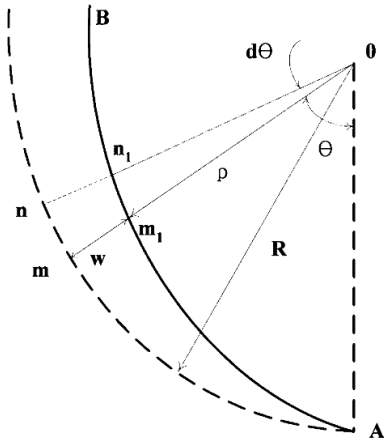

Figure 2- 1 Bending of a Thin Curved Bar (Park et al. 2014)

As shown in Figure 2-1, the initial radius of curvature of the bar was represented by R and the radius of curvature after deformation by ρ. Equation 2-3 presents the relation between the change in curvature and the magnitude of the bending moment M in a thin bar.

$$EI\left(\frac{1}{\rho}-\frac{1}{R}\right)=-M \tag{2-3}$$

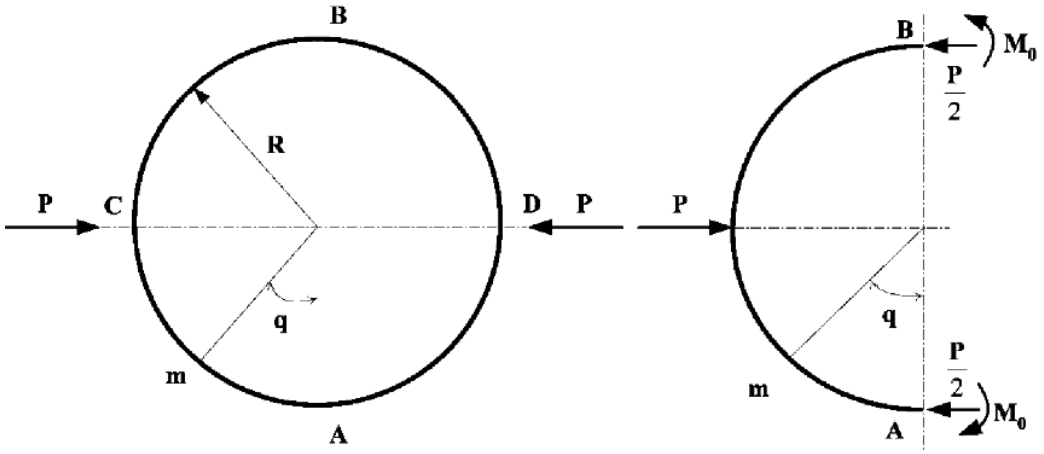

Figure 2- 2 Ring Compression (Park et al. 2014)

A ring of radius R compressed by two forces (P) acting along the diameter similar to a parallel plate loading test set up was considered as presented in Figure 2-2. The bending moment at A and B was denoted by M_o to find the moment at any cross-section as given in Equation 2-4.

$$M = M_0 + \frac{PR}{2}(1 - \cos\theta) \tag{2-4}$$

The bending moment M_o was found using Castigliano's theorem. The strain energy (U) for a thin ring was obtained and is given below in Equation 2-5.

$$U = \int_0^{2\pi} \frac{M^2 R\, d\theta}{2EI} = \frac{2R}{EI} \int_0^{\frac{\pi}{2}} M^2\, d\theta \tag{2-5}$$

The expression for radial deflection at any point was found by solving Equation 2-5 using Equation 2-4.The elongation of diameter AB and the contraction of diameter CD at $\theta = 0$ and $\theta = \pi/2$ respectively were determined as given in Equations 2-6a and 2-6b.

$$\overline{AB} = \frac{PR^3}{4EI}\left(\frac{4}{\pi} - 1\right) \tag{2-6a}$$

$$\overline{CD} = \frac{PR^3}{4EI}\left(\pi - \frac{8}{\pi}\right) \tag{2-6b}$$

The ring stiffness based on vertical and horizontal deflections respectively are presented in Equations 2-7a and 2-7b.

$$\frac{P}{\Delta y} = PS = 6.72\frac{EI}{R^3} \tag{2-7a}$$

$$\frac{P}{\Delta x} = 7.32\frac{EI}{R^3} \tag{2-7b}$$

Park et al. (2014) conducted an FE analysis using ANSYS Ver 11. The model was generated in AutoCAD 2008 and was imported to ANSYS for test simulation. The PS found from all three methods are presented in Table 2-2. Since there is less than 10% discrepancy amongst the three PS's obtained, the author concluded by suggesting that either methods could be used to find PS for preliminary design of pipes.

Table 2- 2 Comparison of PS (Park et al. 2014)

	Vertical Ring Deflection Δy (%)	Experimental Result ①	Theoretical Result ②	FEA Result ③	Difference (%)	
		PS (kN/m²)	PS (kN/m²)	PS (kN/m²)	(①-②)/①x100	(①-③)/ ①x100
GFRP pipe	5	718.4	776.7	726.0	-8.1	-1.1

Campaner et al. (2010) calculated the PS of a jute and glass FRP composite pipe fabricated using a cardanol based matrix and compared their results. The matrix was an epoxy resin which was crosslinked with a cardanol based novolac containing 35% (by weight) unreacted cardanol. On distilling Cashew Nut-Shell Liquid (CNSL), cardanol which is a natural phenol was obtained.

To fabricate the pipes, jute fibres from twisted yarns with a linear density of 270 TEX and HiPer-Tex E-glass fibres with a linear density of 1200 TEX (1 TEX = 1 g/1000 m) were used. The matrix was employed with a catalyst - 2,4 EMI (2-ethyl-4-methyl-imidazole). The pipes had a liner coating which was manufactured using a C glass veil and a glass mat. Once the pipes were manufactured, they were tested using dynamometer (LLOYD LR30K) with a 5 kN capacity load cell according to ASTM D2412 and ASTM D3039 standards. The plates were compressed against the pipe which had a length and diameter of 150 mm at a speed of 12.5 mm/min (Campaner et al. 2010).

STAR-COMPOSITE, a composite design software which works based on classical micromechanics equations and macro-mechanic lamination theory was used to conduct a preliminary design of the two types of pipes. A working pressure of 6 bar was set to design the pipes which were intended to be used for low pressure water transport applications. The fiber and matrix properties, winding angle, pipe thickness and loads corresponding to the working pressure were used to determine the pipe modulus along axial and hoop directions. The fiber properties of jute were determined by the authors in a previous study and was

directly used in this design. The circumferential and axial modulus of the jute composite were found to be 7.15 GPa and 3.18 GPa, respectively. The circumferential and axial modulus of the glass composite were found to be 14.72 GPa and 5.98 GPa. The input data for the software are presented below in Table 2-3 (Campaner et al. 2010).

Table 2- 3 Input Data for STARCOMPOSITE Software (Campaner et al. 2010)

Fibre mechanical properties	Young Modulus (GPa)		Tensile Strength (MPa)	
	Jute	Glass	Jute	Glass
	38	75	380	2800
Matrix mechanical properties	Young Modulus (GPa)		Tensile Strength (MPa)	
	1.7		35	
Fibres (%v)	Glass reinforced pipes		Jute reinforced pipes	
	33		56	
Pipe thickness (mm)	5			
Winding angle (°)	55			
Axial load per unit length (N/m)	22500			
Circumferential load per unit length (N/m)	50000			

The hoop mechanical properties of the composite pipes were measured while testing them under parallel plate compression loading. The specimens were compressed in a direction perpendicular to their axis between the two parallel plates until they reached 30% of their initial diameter. Since the shape of the pipes under loading did not remain constant and started ovalizing, it was necessary to apply a proper correction factor to the PS formula as given in ASTM D2412. This formula with correction factor is presented in Equation 2-8

$$PS = \frac{F}{\Delta y}\left(1 + \frac{\Delta y}{2d}\right)^3 \qquad (2\text{-}8)$$

where d is the internal diameter of the pipe.

The new pipe stiffness was then calculated and compared against the old pipe stiffness as shown in Figure 2-3. It can be seen that the corrected stiffness reaches a plateau after an initial decrease. The pipe stiffness was calculated at 5% and 10% of the vertical diametrical

deformation according to ASTM D2412 standards. The corrected pipe stiffness was used to calculate the flexural modulus (E_{flex}) of the pipe using the formula given below

$$E_{flex} = 0.149\left(\frac{PS \times r^3}{t^3 / 12}\right) \quad (2\text{-}9)$$

where t is the thickness of the pipe and r is the internal radius of the pipe.

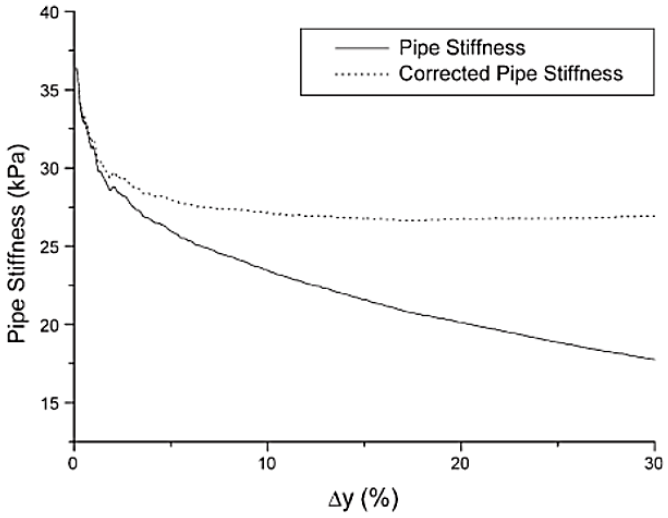

Figure 2- 3 Initial PS and Corrected PS Curves (Campaner et al. 2010)

The tensile modulus calculated for jute and glass FRP samples were found to be 3.5 $\pm$ 0.3 GPa and 7.1 $\pm$ 1.4 GPa, respectively.

Table 2-4 gives the results of the parallel plate test. The values of properties corresponding to the glass reinforced pipes were much higher than that with the jute reinforcement. This was because of the lower modulus and lower fiber content in jute reinforced pipes in comparison to the glass reinforced pipes. Although the values were significantly different, the PS values for both were in accordance with the American Water Works Association (AWWA) and hence could be used for the intended purpose. The specifications suggested a minimum stiffness of 248 KPa for pipes with an internal diameter of 150 mm (Campaner et al. 2010).

Table 2- 4 Results from Parallel Plate Loading Test (Campaner et al. 2010)

Pipe	Pipe Stiffness (KPa)		E_{flex} (GPa)	Fibre content (% volume)
	5%	10%		
Jute/epoxy resin	325 ± 28	296 ± 36	2.0 ± 0.25	33
Glass/epoxy resin	1135 ± 42	1129 ± 22	6.8 ± 0.34	56

2.2.3 Sandwich Pipes under Transverse Compression

Rafiee and Habibagahi (2018) worked on finding the stiffness of a GFRP sandwich composite pipe which was subjected to transverse loading. The ovality occurring in pipe cross section as it is being loaded was considered an irregularity that would reduce the moment of inertia across the cross section. The induced higher stress when compared to the stress experienced in a perfectly circular cross section would compromise the mechanical integrity of the pipeline. Moreover, the pipe ovalization would disrupt the fluid transmission and affect the performance of the pipe. Consequently, estimating and analyzing the stiffness of pipes during the design stages and prior to the mass production was critical from both structural and functional point of view.

The focus of this research was to estimate the apparent ring stiffness of the GFRP sandwich pipe using a simple analytical approach and FEA. Test specimens used for this study were 300 mm in length and 500 mm in diameter, cut from a full-length GFRP sandwich pipe. The specimens were made of glass/polyester composite manufactured using discontinuous filament winding process. The specimens also consisted of a liner layer and structural plies. The liner of 1.5 mm thickness was composed of surface mat, stitched glass fiber and polyester resin to protect the structural layer from direct exposure to the internal fluid. The liner was to provide a smooth internal surface for transmission of fluid with minimum head loss from hydraulic viewpoint. The ply configuration [90/±60.19/ Core/ ±60.19/90] of the structural layers was a combination of hoop/cross plies and a core layer.

Composite made of E-Glass direct roving and polyester resin was used for both hoop and cross plies. The core layer was an impregnated industrial sand filler with polyester resin. The overall pipe thickness was 6.06 mm with the thickness of hoop, cross and core layers being 0.76, 2.64 and 1.16 mm, respectively (Rafiee and Habibagahi 2018).

Solely increasing the GFRP pipe-wall thickness by adding extra redundant GFRP layers was to lead to an overdesigned pipe and would have led to an unfeasible overall product cost. Hence, a sand/resin layer was introduced to increase the pipe thickness and enhance the pipe stiffness as shown in Figure 2-4.

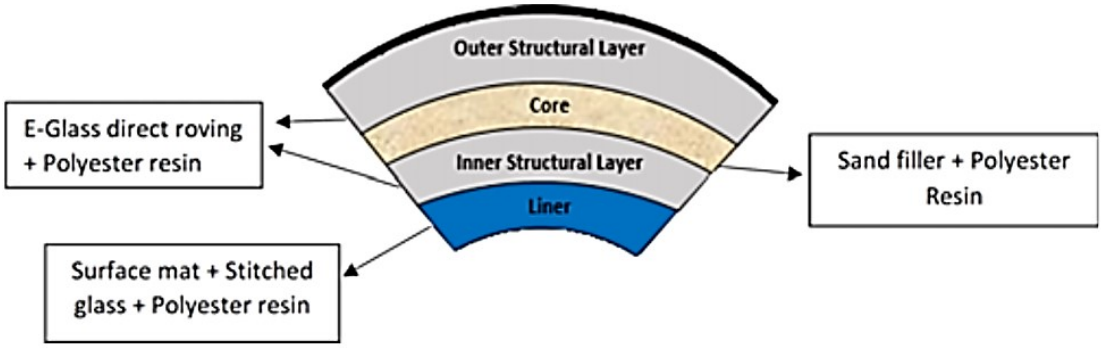

Figure 2- 4 Schematic Presentation of GFRP Sandwich Pipe Wall Construction (Rafiee and Habibagahi 2018)

The mechanical properties of materials used for this study are presented in Table 2-5. Using three samples taken from the pipe, weight fraction was found using ASTM D 3171-06 Procedure G – Method 1 and are presented.

Table 2- 5 Mechanical Properties of Pipe (Rafiee and Habibagahi 2018)

	Glass Fiber	Polyester Resin	Silica Sand
Young's modulus [GPa]	70	3.5	10
Poisson's Ratio	0.22	0.33	0.39
Tensile Strength [MPa]	1970	78	-
Compressive Strength [MPa]	-	130	-
Weight fraction [%]	59.5	31.1	9.4

Three specimens were tested under parallel plate loading using a Universal Testing Machine (UTM). The specimens were compressed until the diametric deflection reached 5% of the vertical diameter, at a constant rate of 12.5 ± 2.5 mm/min. On unloading, the specimen retained its original shape without experiencing any permanent deformation confirming that the specimen was within the elastic region till it reached 5% diametric deflection. No visual cracking, delamination or rupture was observed. A pipe stiffness of 163.3 KPa was recorded at 5% deflection which corresponded to a compressive load of 1.225 kN. On continuing the test further, it was observed that the specimen experienced failure at 7.078 kN which corresponded to 33% diametric deflection (Rafiee and Habibagahi 2018).

Rafiee and Habibagahi (2018) used a similar approach as Park et al. (2014) to obtain the PS by using the 2-D ring concept. Although, since the pipes tested by Rafiee and Habibagahi (2018) had layers with different materials it was essential to use an appropriate moment of inertia (I). The cross section of the GFRP sandwich pipe wall was similar to an I beam. Each layer had a different elastic modulus based on its fiber direction as presented in Figure 2-5 and the equivalent modulus of the cross section had to be calculated.

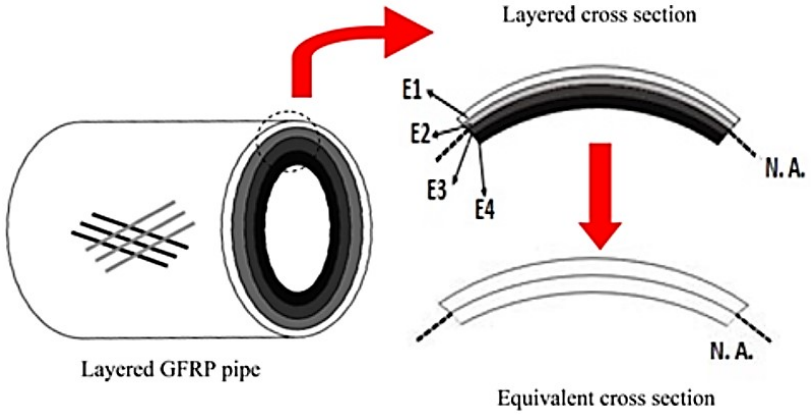

Figure 2- 5 Equivalent Cross Section of GFRP Sandwich Pipe (Rafiee and Habibagahi 2018)

Using equations of micromechanics, expressions for longitudinal modulus (E_X), transverse modulus (E_Y), in-plane shear modulus (E_S) and major Poisson's ratio (ν_X) was formulated using fiber modulus (E_f), matrix modulus (E_m), fiber in-plane shear modulus (G_f) and matrix in-plane shear modulus (G_m). The in-plane mechanical properties of GFRP sandwich pipe layers, i.e. E_X, E_Y, E_S and ν_X, were fed into a transformation equation to obtain the young's modulus of each ply along hoop direction and the location of neutral axis with respect to centerline was found. The PS of GFRP sandwich pipe was calculated based on the geometrical specification of cross-section and mechanical properties of the constitutive layers as given in Equation 2-10 (Rafiee and Habibagahi 2018).

$$PS_{thr} = \sum_{i=1}^{\text{last ply}} \frac{E_H^i \times \bar{I}^i}{0.149(R^i + NA)^3} \tag{2-10}$$

Finite element analysis using the commercial software Abaqus was conducted. Two types of 3-D FE models were generated using the conventional and continuum shell elements. A numerical analysis was performed under displacement control conditions. The upper plate was given a displacement of -25 mm in y direction, while the other plate was fixed in all directions and the reaction forces were measured. Since large deformations were encountered during the analysis, geometric non-linearity feature was turned on in the software. Though the fiber behavior was linear, the resin behavior was non-linear. Hence, material nonlinearity associated with inelastic behavior of the composite materials were also considered. These three sets of FEA were done on both the models for comparison:

1. A completely linear analysis.
2. Non-linear geometry and linear material behavior considered.
3. Both geometrical and material non-linearity considered.

Table 2- 6 Comparison Between Theoretical Modeling and Experimental Observation and FEA (Rafiee and Habibagahi 2018)

	Conventional shell element			Continuum shell element			Theoretical analysis	Experiment
	A*	B**	C***	A	B	C		
Reaction force [N]	1745.6	1267.8	1260.5	1603	1242	1239	976.27	1225
Stiffness [KPa]	232.7	169.04	168.06	213.7	165.6	165.2	130.17	163.3
Error	42.5%	3.5%	2.9%	30.8%	1.4%	1.1%	-20.8%	-

*A: Linear model
**B: Linear material behavior and nonlinear deformation
***C: Nonlinear material behavior and nonlinear deformation

On comparison, the theoretical calculation underestimates the stiffness of pipe which often leads to over designing. The difference in stiffness occurred as the effect of non-linearities, pipe curvature and influence of wall thickness were not considered. The author concluded that using description of materials layer-wise is essential and the use of equivalent one-layer properties should be avoided.

2.2.4 Geometric Non-Linearity in Pipes under Transverse Compression

On being subjected to transverse compression, FRP liners start failing elliptically and undergo large deformations. This causes a non-linear load – displacement response in the pipe. While analyzing flexible structures like these, a typical linear elastic analysis may not adequately capture the true response of the structure. Deflections are assumed to be small relative to size of the member, i.e. there is a comparatively small difference between the undeformed and deformed shape of the structure, in a linear elastic analysis. The static equilibrium equations for these are based on the undeformed geometry and the strains are linear functions of the displacements, resulting in linear equilibrium equations. However, when the displacements become large, it is essential to consider the effects of geometric stiffness in order to obtain results that are accurate and physically representative. It is a function of the internal force in an element and the change in position of its nodes. In order for a structure to remain in static equilibrium as it undergoes finite deformations, forces

are developed within the members to balance externally applied force. When these internal forces are caused by the change in geometry, there is an increase in the stiffness. This is known as stress stiffening or geometric stiffening. It is more accurate to refer to the static equilibrium equations to the deformed configuration while solving for structures of this nature. The strain – displacement functions are non-linear, resulting in non-linear equilibrium equations. This kind of problem is called geometrically non-linear (Lebofsky 2013). Hence, it was important to consider geometric non-linearity while analyzing the FRP liners which were subjected to transverse compressive loading to compare against the experimental results in this study.

2.2.5 Long Term Ring Deflection of Buried Pipes

Kim et al. (2019) studied about the long term ring deflection of pressurized buried pipes as the PS reduced over time. A large diameter sandwich pipe was constructed from reinforced polymer mortar pipe (RPMP) which was embedded between fiberglass pipes. The diameter of the sandwich pipe was 2400 mm and it was buried for 664 days. FEA and pipe ring deflections predicted using the Iowa formula in AWWA M45 was used to determine the safety of the buried pipe. The long-term behavior of the pipe was determined statistically using initial ring deflection data according to ASTM D5365 to predict the long term ring deflection. The structural behavior of a buried pipe is dependent on the external pressure acting upon it. The vertical earth pressure acting on the buried pipe can be determined from the load on the top of pipe and loaded area when a static load is acting on it. In this case, there was an induced earth pressure in the horizontal direction as the buried pipe deformed. The vertical earth pressure generated from the applied load became greater than the horizontal earth pressure caused by the pipe deflection.

When a pre-load was applied to the pipe without considering the effect of the surrounding soil on the pipe deflection, the pipe deflections were calculated using Equation 2-7a and 2-7b (Kim et al. 2019).

The Iowa formula in ASTM D2412 was also used to predict the deflection of flexible buried pipes as given in Equation 2-11.

$$\Delta_h = \frac{(D_L W_C + W_L)K_X}{0.149PS + 0.0061E'} \quad (2\text{-}11)$$

where , D_L = Deflection lag factor

W_C = Vertical soil load on the pipe (N/m^2)

W_L = Live load on the pipe (N/m^2)

K_S = Bending co-efficient

E' = Composite soil constrained modulus

The Iowa formula limits the deflection to 5% for the safety of the pipes and prevent leakages. For the test, the pipes were buried and the soil over it was compacted. The vertical and horizontal deflections were measured using a laser distance meter. A Finite Difference Analysis (FDA) was conducted using the program MIDAS/GTS to compare it against the experimental test results. Three burial depths – 5 m, 10 m and 16 m, three domains and soil characteristics based on the pipe bedding material were considered for this analysis. The results from the experimental and FDA analysis are given in Table 2-7. Case 1 was in closer agreement with the test data and it was found that compaction density of the pipe affected the deflection levels (Kim et al. 2019).

The vertical and horizontal deflections at 1 m, 3 m, and 5 m from the entrance of the pipe were measured. The pipe deflection was within 1.5% of the original pipe diameter. It was found that majority of the deflection occurred within the first 30 days of construction. In

the buried condition, the pipe began deflecting elliptically and experienced a reduction in the vertical diameter and increase in horizontal diameter. The deflection – time graphs are presented in Figure 2-6.

Table 2- 7 Comparisons of Numerical Analysis and Experimental Results (Kim et al. 2019)

Buried depth (m)	Two-dimensional analytical results (%)						Experimental results (%)		AWWA M45 (%)	
	Case 1		Case 2		Case 3					
	Δ_v	Δ_h	Δ_v	Δ_h	Δ_v	Δ_h	Δ_v	Δ_h	Δ_v	Δ_h
5	−0.28	0.27	−0.75	0.71	−1.17	1.18	−0.17	0.17	−0.52	0.52
10	−0.56	0.53	−1.38	1.30	−2.06	2.07	−0.38	0.38	−1.05	1.05
16	−0.90	0.85	−2.13	2.00	−3.08	3.09	−0.71	0.54	−1.67	1.67

Note: (+): increases in diameter; (−): decreases in diameter.

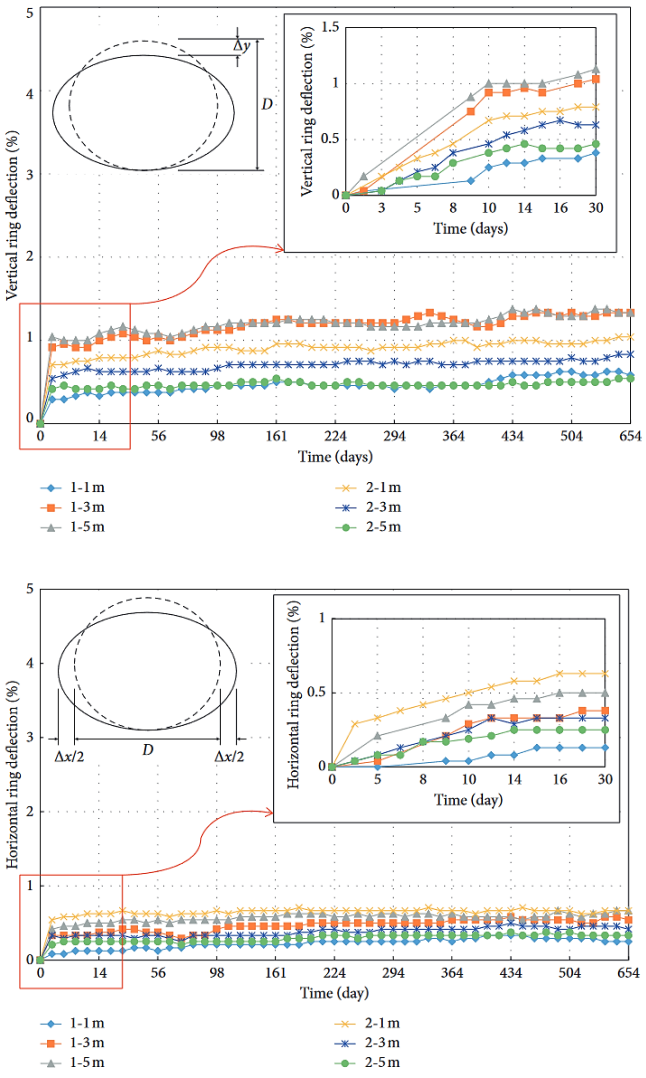

Figure 2- 6 Field Test Results of Deflection vs. Time (Kim et al. 2019)

The authors concluded that the effect of PS on deflection was minimal and was within 3.5% deformation. At that stage, the contribution of soil foundation and PS to the deflection was about 96.5%. Hence, the authors suggested that the soil foundation could play a major role in deflection levels of buried pipes (Kim et al. 2019).

2.3 Advantages of using FRP Sandwich Composite Pipes

Generally, the compressive strength of FRP elements are lower than their tensile strength. Also, thin FRP sheets have less stiffness which leads to installing layer after layer of fabrics inside a pressure pipe to obtain a liner of sufficient thickness and adequate stiffness. In such repairs, it is common to see designs calling for 12 or more layers of fabrics. The typical cost of a single layer of CFRP with installation charges is about $300 per square meter in the US. Accordingly, a 12-layer system would cost over $3500 per square meter of the pipe surface area. The major shortcomings of this system are both the high cost of repair and the long installation time. Also, since many of these repairs are to be performed with a shutdown and under tight schedules, shortening the repair time is of extreme importance to the owners of these pipes running power plants, water utilities, etc. Sliplining a conventional pipe into the deteriorated pipe is a commonly used technique. However, this often causes a significant loss in flow capacity of the repaired system due to the large annular space it creates between the host pipe and the new pipe. The above shortcomings led to the development of the StifPipe® which is FRP sandwich pipe by Ehsani (2019). There are two engineering attributes that the structure of a pipe must offer:

1. Sufficient strength and stiffness while being handled during installation and in resisting gravity loads safely.

2. Adequate strength to resist the internal fluid pressure in both hoop and longitudinal directions.

Ehsani (2019) addressed these by making a new sandwich pipe that uses GFRP or CFRP skin and a light-weight honeycomb panel core. The interior surface of the pipe was to be coated with CFRP to resist hoop stresses and thrust loads. It was advantageous to use the anisotropic property of FRP as the tensile strength of FRP is dependent on the direction of the fibers. The fibers oriented in the hoop direction was to resist internal pressure and the fibers positioned along the length of the pipe was to provide resistance against thrust. This feature of FRP helps to come up with an economical design. The thickness and rigidity of the pipe could be increased at a low cost by using a spacer material such as a light-weight honeycomb core or 3D fabric. The sandwich pipe would resemble the flange-web system of an I-beam.

Ehsani (2019) demonstrated the following using a sandwich panel system:

- Thickness of 1 layer of CFRP fabric = 1.3 mm
- Thickness of 1 layer of honeycomb core = 7.5 mm
- Total thickness of the panel = 10 mm

The stiffness of the panel was increased to 37 times while there was only a 9% increase in weight on introducing a spacer.

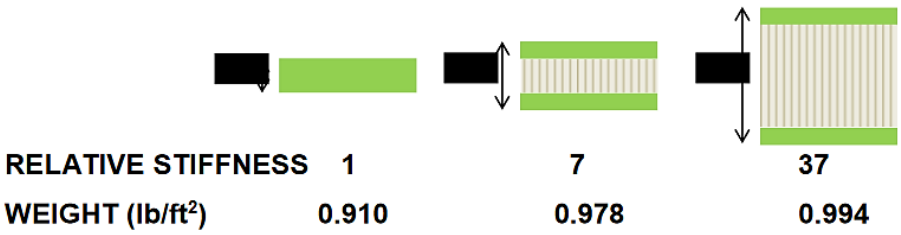

Figure 2- 7 Comparison of Stiffness of CFRP with CFRP as Skin Reinforcement to a Lightweight Polypropylene Honeycomb Core (Ehsani 2019)

The pipe could be designed for any internal pressure by adding additional layers of CFRP to the inner surface of the pipe. A light-weight and inexpensive spacer like polypropylene honeycomb or 3D fabric was to provide stiffness to the pipe. To increase the stiffness and provide durability against environmental conditions, FRP fabric layers were provided externally. FRP being non-corrosive eliminated the need for cathodic protection. It weighed 10% - 15% of a conventional GFRP pipe and is significantly lighter than steel or concrete pipes (Ehsani 2019).

Ehsani (2019) has reported a real time application of this sandwich pipe for the rehabilitation of a pressure pipe. The Aguirre power plant in Puerto Rico had a large network of pipelines ranging from 600 to 1500 mm in diameter, delivering cooling water to various parts of the plant or carrying the used water to be discharged in the Caribbean Sea. These pipes operated at a pressure of about 1-1.4 MPa (150-200 psi). The access to the pipe network was through the riser pipes. Due to severe corrosion in one of these riser pipes, the steel cover dislodged under pressure. The pipe lid was thrown nearly 30 m away from its location. Consequently, all the pipes were inspected, and it was found that several risers exhibited various degrees of corrosion near the ground level. It was decided to repair the upper 1.2 m of 29 riser pipes. There was a concern to repair these 36-inch diameter steel pipes coated with a cementitious mortar lining expeditiously.

The pipes were subjected to:

1. Internal fluid pressure
2. External load from the weight of the soil and traffic

On evaluation, a full structural repair (Class IV) to resist these loads without being reliant on the host pipe was planned. There were three design alternatives:

1. Replace the upper 1.2 m of the riser pipes with a new steel pipe.
    a. Excavation around the riser was required. Had to provide temporary shoring for the surrounding soil. The existing pipe had to be cut and removed.
    b. Installation and welding of new pipe to the old pipe and coated with mortar.
    c. Removal of shoring and backfilling.

This conventional repair technique was ruled out as it required more time to complete and would have caused a disruption of service.

2. Repair the pipe with CFRP using the wet layup technique. This technique has proven to be successful in the repair of similar steel pipes (Geraghty 2011).
    a. If only the internal pressure of the pipe was to be considered, then one or two layers of CFRP would have been sufficient.
    b. Since external loads were also to be considered in this case, design called for 6 to 7 layers of CFRP as it was controlled by the stiffness or rigidity of the liner.

This option was time-consuming and expensive. High chances of lower quality installation was possible as the entire repair had to be performed in the field. Skilled labor was also not readily available on the island.

3. Using StifPipe® made of GFRP/CFRP skin and a honeycomb/ 3D fabric core.
    a. Easily manufactured, stored and transported before the shutdown and installed quickly.

On analyzing the three alternatives, this was the most feasible technique to carry out the structural repair of the 29 riser pipes (Ehsani 2019). The pipe had to be designed for an internal pressure of 2.75 MPa (400 psi), which is considerably higher than the operating

pressure of 1.03 MPa (150 psi) and had to be freestanding to resist the external traffic and soil weight loads. The deteriorated riser pipes coated with a cementitious mortar had a diameter of 914 mm. For rehabilitation, the sandwich pipe of 890 mm outer diameter was chosen to fit inside the host pipe and the annular space was to be filled with grout. The major advantage of this sandwich pipe is its ability to be manufactured to fit a pipe of any shape and size (Ehsani 2019).

The sequence sandwich pipe layers from inside to the outside of the deteriorated pipe wall as presented in Figure 2-8:

- 1 Layer of chopped strand mat
- 2 Layers of TU27C (Unidirectional Carbon Fabric)
- 1 0.31-inch spacer sheet
- 2 Layers of VB26G (Biaxial Glass Fabric)

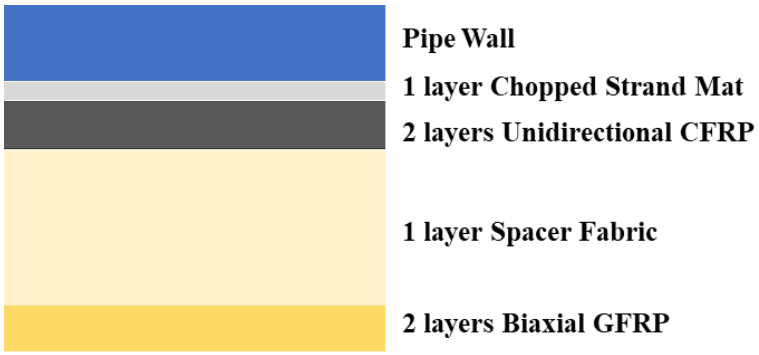

Figure 2- 8 Cross-Sectional View of Sandwich Liner proposed by Ehsani (2019)

Each layer served a particular function as given below:

1. To provide an impervious layer that covers all small pinholes present in the pipe surface, chopped strand mat richly saturated with resin was used.
2. The 2 layer unidirectional CFRP was to provide hoop strength that would help resist an internal pressure of 2.75 MPa (400 psi) with an adequate factor of safety.

3. The spacer fabric was to increase the moment of inertia of the cross section by acting as the web of an I beam and also to increase the rigidity of the pipe.
4. The longitudinal fibers of the biaxial glass fabric was to increase the hoop strength and ring stiffness of the pipe. The fibers in the transverse direction were to increase the strength of the pipe along its length.

The overall weight of a 1.2 m long sandwich pipe that was used to rehabilitate 29 riser pipes was only 36 kg. Two pieces of the sandwich pipe were randomly selected from the production line and were tested under parallel plate testing according to ASTM D2412 as part of quality control and to verify the validity of design assumptions. The behavior of the sandwich pipes were linear to failure as presented in Figure 2-9. The load – deformation behavior of the two samples were identical within the elastic range indicating a high quality of construction. The ring stiffness was calculated for both samples and averaged at different deflection levels as presented in Table 2-8. This could be used in the design of pipes subjected to external compressive loads as the results were comparable with HDPE and PVC pipes (Ehsani 2019).

The dashed curve in Figure 2-9 is the result of a test conducted by the author Ehsani (2012), in which a 914 mm diameter pipe with 6 layers of a high strength unidirectional carbon fabric was tested under transverse compression. A significant increase in stiffness can be noted though the sandwich pipe had lesser number of fabric layers when compared to the solid wall composite pipe which was made of 6 carbon fabric layers. This data proves that using a sandwich pipe is highly economic and it also has a higher stiffness capacity (Ehsani 2019).

Table 2- 8 StifPipe® Stiffness at Different Deflection Levels (Ehsani 2019)

Percentage of outside diameter	3%	5%	8%	10%
Deflection mm (inches)	28.4 (1.12)	47.2 (1.86)	75.7 (2.98)	94.7 (3.73)
Pipe Stiffness for Sample # 1 kPa (psi)	136 (19.7)	133 (19.3)	127 (18.4)	121 (17.6)
Pipe Stiffness for Sample # 2 kPa (psi)	148 (21.5)	141 (20.5)	132 (19.2)	127 (18.5)
Average of two Samples kPa (psi)	142 (20.6)	137 (19.9)	130 (18.8)	124 (18.0)

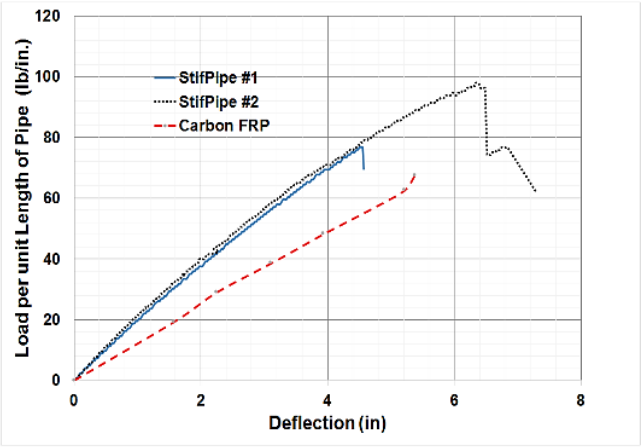

Figure 2- 9 Load-Deflection Results of the Sandwich Pipe (Ehsani 2019)

2.4 INFERENCE FROM THE LITERATURE

On reviewing the literature, it was found that various studies on the behavior of solid wall FRP pipes, under axial loading and/or internal hydrostatic pressure (Das and Baishya 2016; Wang et al. 2016), impact loading (Wakayama et al. 2002; Deniz et al. 2013) and fatigue cycles (Tarakcioglu et al. 2007; Rafiee and Elasmi 2017), pipe mechanics and fracture strength (Parashar and Mertiny 2011) etc. have been carried out. Similarly, it is evident that innumerable works have been performed to understand the behavior of sandwich pipes which are mainly being used for under sea and deep-water applications. Studies on shearing capacity, compressive strength and behavior (Liu et al. 2017; Hansen 1998) , temperature field of sandwich pipe (Wang et al. 2017), shear deformation based on bending and buckling (Jianghong 2015), external pressure capacity (Arjomandi and Taheri 2011), elastic buckling and bending capacity (Arjomandi and Taheri 2012; 2010) based on an experimental, analytical and numerical approach, have been performed.

Limited tests to understand the behavior of solid wall FRP liners bonded inside PCCP as a rehabilitative measure, such as sectional ring tests, external load test for three-edge bearing (TEB) strength, full scale hydrostatic burst test, radial compression test (Lee and Karbhari 2005; Rafiee and Habibagahi 2018) have been conducted and a stress analysis (Houssam and Sean 2001) has also been done. Similarly, sandwich pipe liners of a few different facesheet-core-resin combinations have been patented with some providing the method of lining as well (Kittson and Kulawic 1998; Imoto et al. 1993; Aylor Jr. and Hirtz 1990). There are less than five studies in the literature, discussing about the behavior of solid wall FRP and sandwich pipe liners which are subjected to transverse compression. The actual behavior of both solid wall and sandwich FRP liners under this loading are not well known. In many studies, FEA has been used to simulate the effect of parallel plate loading and physical parameters such as the PS and SF of FRP ring specimens have been determined using commercial softwares like ANSYS and ABAQUS. Using FEA reduces the number of physical tests and thereby helps in creating an optimized solution in a short duration of time. However, FEA is the only analysis method that has been currently used to illustrate the material and geometric non-linearity of FRP composite elements. No simple analytics have been developed to substantiate the geometric non-linearity displayed by the liners while largely deforming under loading.

Hence, this research was focused on analyzing the behavior of FRP liner under transverse compression to determine the stiffness and strength parameters. An iterative analytical model was also developed by considering geometric non-linearity and was compared against the test data.

CHAPTER 3 EXPERIMENTAL PROGRAM

The outline of experimental program conducted for testing FRP solid wall and sandwich liner specimens are provided in this section. A test matrix is used to describe the specimen categories. All materials properties are discussed with a detailed explanation and the fabrication and testing procedure is also made available. The failure modes are demonstrated and the test results, including load – deflection behavior and load – strain behavior are presented and discussed.

3.1 TEST MATRIX

For the solid wall liners, GFRP and CFRP specimens with an average outer diameter of 340 mm and width of 315 mm were fabricated. Four layers of fabric with a finishing overlap of approximately 100 mm were cured in epoxy resin for both liner types. For the sandwich liners, specimens with two layers of either GFRP or CFRP facesheets with 100 mm overlap and a 3D woven fabric or a bulkermat core, with an average outer diameter of 350 mm and width of 310 mm were fabricated. The solid wall test specimens were identified with a specimen ID as XY - Z, where X stands for the number of fabric layers and Y stands for either fiberglass (G) or carbon (C) fiber and Z denotes the ID number. For example, 4G – 1 stands for GFRP solid wall specimen with 4 layers of GFRP with ID number 1. The sandwich test specimens were identified with a specimen ID as XY-A-XY - Z, where X stands for the number of fabric layers, Y stands for either fiberglass (G) or carbon (C) fiber, A stands for either 3-D woven fabric (W) or Bulkermat (B) core and Z denotes the ID number. For example, 2G-W-2G - 1 stands for GFRP sandwich specimen with 2 layers of GFRP and 1 layer of 3-D woven core with ID number 1. The test matrix is presented in Table 3-1 and cross-sectional view of specimens are shown in Figure 3-1.

The test matrix was developed to increase the strength and stiffness of solid wall specimens by introducing a spacer fabric. A normalized elastic modulus was found using the coupon thickness of GFRP and CFRP composites, respectively. This was further used to calculate the normalized ring stiffness at different deflection levels to make all the six specimen types comparable. Having a comparable stiffness parameter helps in identifying a potential material for structural rehabilitation.

Initially, a 3-D woven fabric core was introduced as a spacer material. Although the initial stiffness was improved, the strength was compromised. A bulkermat foam core was then introduced to improve both strength and stiffness of the liner system.

Table 3- 1 Test Matrix

#	Specimen ID	Outer Diameter (mm)	Width (mm)	Wall thickness (mm)	Note
1	4G - 1	329.75	309.00	04.53	Glass solid wall
2	4G - 2	343.25	320.13	04.13	
3	4G - 3	338.50	313.00	04.27	
4	4G - 4	344.63	318.38	04.21	
5	4C - 1	347.63	316.38	05.36	Carbon solid wall
6	4C - 2	346.75	315.63	05.17	
7	2G-W-2G - 1	358.38	290.50	11.52	GFRP/3-D woven sandwich
8	2G-W-2G - 2	355.63	308.13	11.65	
9	2G-W-2G - 3	358.00	314.50	11.22	
10	2G-W-2G - 4	358.00	314.75	11.30	
11	2C-W-2C - 1	360.38	315.38	12.14	CFRP/3-D woven sandwich
12	2C-W-2C - 2	361.50	318.50	12.50	
13	2C-W-2C - 3	360.88	318.38	11.79	
14	2C-W-2C - 4	353.50	311.25	12.66	
15	2G-B-2G - 1	345.25	304.75	09.55	GFRP/Bulkermat sandwich
16	2G-B-2G - 2	346.63	303.29	09.77	
17	2G-B-2G - 3	346.88	305.88	09.24	
18	2C-B-2C - 1	345.75	300.88	09.87	CFRP/Bulkermat sandwich
19	2C-B-2C - 2	346.50	304.63	09.87	
20	2C-B-2C - 3	300.75	345.63	10.08	

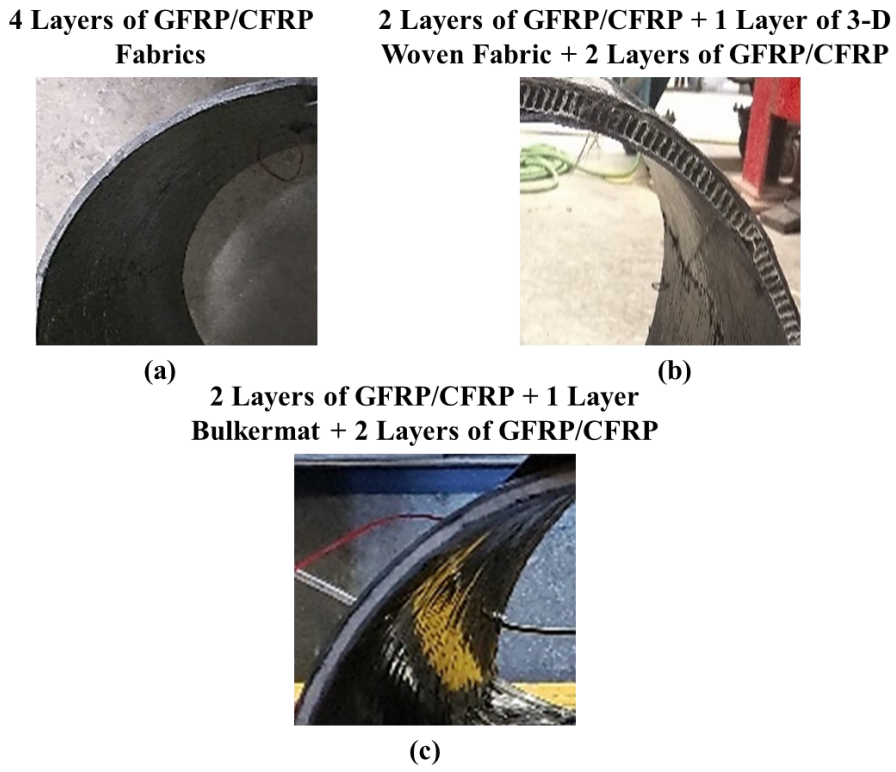

Figure 3- 1 Cross-Sectional View of (a) Solid Wall ; (b) & (c) Sandwich Specimens

3.2 MATERIAL PROPERTIES

For the solid wall liners, unidirectional glass/carbon fabric saturated using a two-component epoxy resin was used. The aerial weight of dry glass fabric was 915 g/m^2. It had a tensile strength of 3.24 GPa, tensile elastic modulus of 72.4 GPa, density of 2.55 g/cm^3 and an ultimate elongation (rupture strain) of 4.5%. A two-component epoxy resin was mixed in a ratio of 2:1, with two parts of resin and one part of hardener. The viscosity of two-component saturating resin was 1500-1600 cps. After the full cure time of 48 hours, the resin is reported to have a tensile strength, compressive strength and flexural strength of 49.3 MPa, 65.4 MPa and 76.8 MPa, respectively. The tensile modulus, compressive modulus and flexure modulus were 1.995 GPa, 3.25 GPa and 1.740 GPa, respectively. Also, the water absorption was < 1% in 24 hours. When the glass fabric was laminated

with epoxy, the nominal ply thickness was 1.3 mm. McCracken and Sadeghian (2018) performed the tensile test and the results based on nominal ply thickness of 1.3 mm for an average tensile strength was 583 ± 31 MPa and the average elastic modulus was 21.75 ± 0.58 GPa. The test procedure and results are presented in Appendix B. The dry carbon fabric had a weight of 943 g/m^2, tensile strength of 3.8 GPa, tensile modulus of 231 GPa, density of 1.8 g/cm^3, ultimate elongation of 1.64%. When laminated with epoxy, the carbon fabric had a ply thickness was 1.24 mm. The CFRP laminate had an average tensile strength of 1126 MPa and an elastic modulus of 100 GPa. For the sandwich liner, the GFRP and CFRP facesheets had the same properties as mentioned above.

The core was composed of 3-D woven fabric made with two bi-directionally woven glass fabrics, mechanically integrated with vertical woven piles. One pillar had two S-shaped piles and appeared in shape of 8 and 1 from the warp and weft direction, respectively. The dry aerial weight and thickness of the core were 1050 g/m^2 and 8 mm, respectively. The density in warp direction was 15 ends/cm and density in weft direction was 8 ends/cm. The tensile strength in warp and weft directions were specified to be 6000 N/50 mm and 10000 N/50 mm, respectively. Based on preliminary tests conducted by McCracken and Sadeghian (2018), the average thickness after curing was found to be 7.54 mm and the weight of the fabric was 2988 ± 134 g/m^2. Bulkermat is a low density, nonwoven continuous-strand laminate bulker/print control mat constituting of micro balloons (45% by weight). It has a density of 0.045 g/m^3, dry aerial weight of 160 g/m^2 and dry thickness of 4.1 mm. The tensile strength and elastic modulus in longitudinal and transverse directions were 6.37 and 5 MPa, and 1.19 and 1 GPa, respectively.

Material properties of dry fiber, epoxy and core material are as specified by the manufacturer QuakeWrap Inc., Tucson, AZ, USA. Facesheet laminate and core material properties are given in Table 3-2.

Table 3- 2 Facesheet and Core Material Properties

GFRP Laminate	
Ply Thickness (mm)	1.3
Avg. Tensile Modulus (GPa)	21.75
Avg. Tensile Strength (MPa)	582.93
Avg. Rupture Strain (mm/mm)	0.0274
CFRP Laminate	
Ply Thickness (mm)	1.24
Avg. Tensile Modulus (GPa)	100
Avg. Tensile Strength (MPa)	1126.35
Avg. Rupture Strain (mm/mm)	0.0115
3-D Woven Fabric	
Young's Modulus (MPa)	57
Core Shear Modulus (MPa)	16.6
Bulkermat	
Young's Modulus (MPa)	374.4
Core Shear Modulus (MPa)	144
Ultimate Shear Strength (MPa)	2.2

3.3 Specimen Fabrication

The following procedure was adopted for specimen fabrication:

Step1: To fabricate the liner specimens, sheets of glass and carbon fabric and, the 3-D woven fabric and bulkermat core were cut to required length using shears. Having scaled and cut the fabric requirements to a larger dimension helped in fabricating 3 or 4 liners at once. Wet lay-up method was used to fabricate all the specimens.

Step 2: The fabric was thoroughly cleaned of any minute dust particles.

Step 3: A plastic sheet was used to cover the cardboard mandrel of 305 mm nominal diameter, before placing the fabric.

Step 4: For the solid wall liners, a layer of resin was applied on the plastic sheet for good bonding and then four layers of glass or carbon fabric was wrapped around while sufficiently wetting the fabric with epoxy and providing an end overlap of 100 mm. Similarly, for the sandwich liners, 2 layers of glass or carbon fabric were applied as inner and outer facesheets and one layer of 3-D woven fabric or bulkermat were applied as the core material of the liners.

Step 5: A roller was used to evenly distribute the resin over the fabric surface and a spatula was used to smoothen the resin layer.

Step 6: A motor system was used to spin the mandrel slowly to create a small centrifugal force in order to avoid the concentration of the resin at the bottom as shown in Figure 3-2.

Step 7: The specimens cured for approximately 24 hours at room temperature with a plastic sheet covering its exposed surface, to obtain a smooth and dust free surface.

Step 8: The cardboard mandrel and plastic sheets were removed, and the liner was allowed to cure.

Step 9: After at least 7 days of curing at room temperature, the single unit of liner was cut into three or four identical specimens using a diamond-bladed saw. The rough edges were sanded to obtain a smooth surface.

Step 10: A measuring tape was used to measure the outer diameter and width, and a digital caliper was used to measure the thickness of each specimen at eight different locations and was averaged for further calculations.

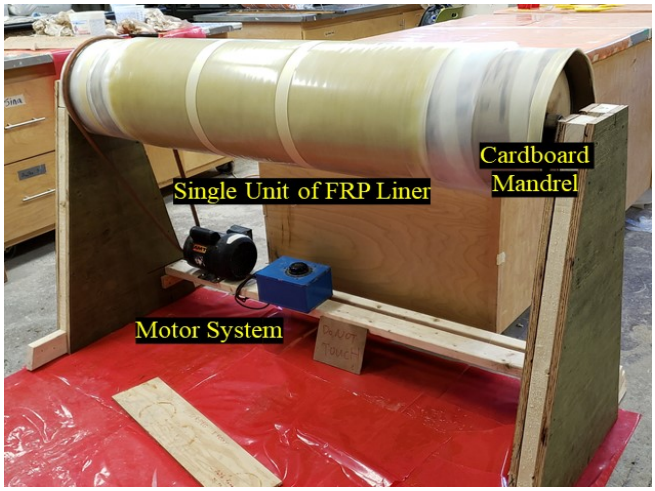

Figure 3- 2 Specimen Fabrication

3.4 Test Setup and Instrumentation

For testing the liners, a customized parallel-plate load test setup was crafted using a 20 kN load cell. The plates were 450 x 750 mm in size and had a thickness of 12.7 mm. The stroke of actuator was 340 mm and pump allowed a loading rate of 20 mm/min. For the liners, two strain gauges (SG) were applied at mid-height of the liner on the crown and invert positions. Two strain gauges were applied on either exterior side of the liner at springline position as shown in Figure 3-3. All strain gauges were placed parallel to the fiber direction. The fabricated specimen was connected to a string potentiometer on sides A and B by drilling small holes on either side of the liners, which could measure up to 635 mm deflection in the horizontal direction. Likewise, string potentiometers C and D were clamped to top and bottom plate respectively and could measure a deflection of up to 305 mm in the vertical direction. All the specimens were then tested under compressive transverse loading according to ASTM D2412-11 (2018) standards. Displacements in vertical and horizontal directions and strains in springline and crown/invert positions were collected using a data acquisition system (DAQ) with a frequency of 10 Hz and were further processed for analysis.

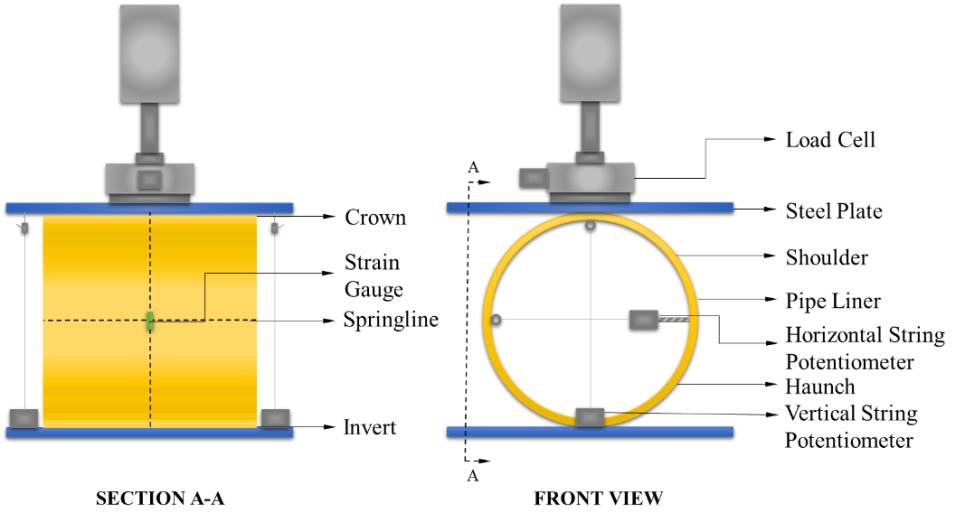

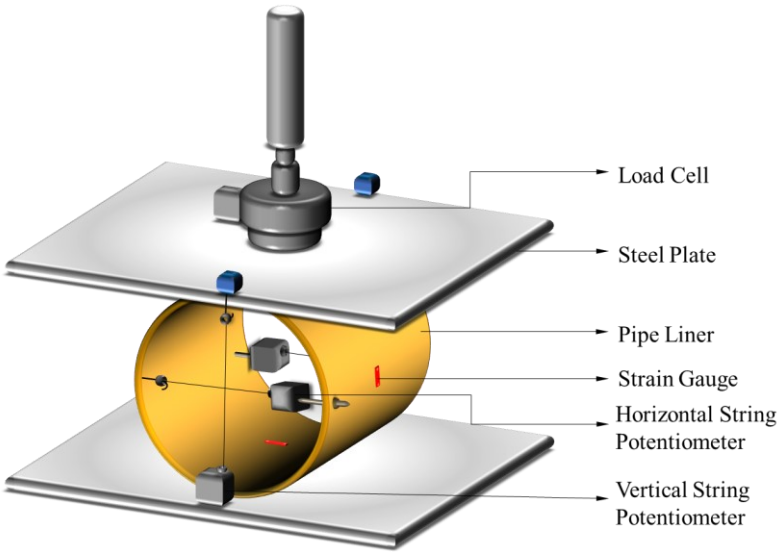

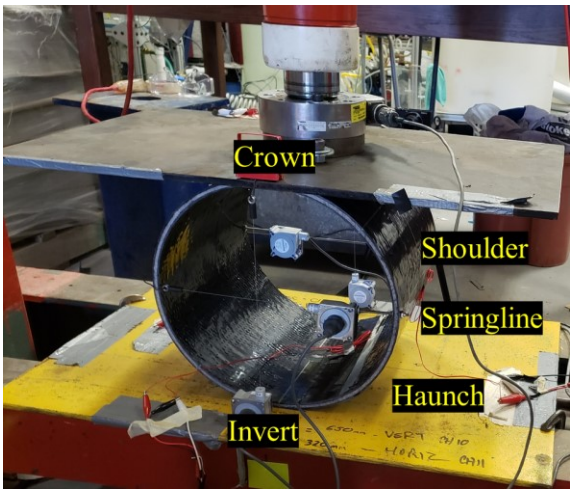

Figure 3- 3 Test Set-Up and Instrumentation

3.5 Experimental Results and Discussion

3.5.1 Failure Modes

3.5.1.1 Solid Wall Liners

The common failure mode that GFRP solid wall liners experienced was wall crushing at springline. Specimens 4G - 3 and 4G - 4 delaminated at the crown and underwent wall buckling. The modes of failure for GFRP liners are presented in Figure 3-4. Cracking was initiated at the springline at around 5 kN for all the four specimens. The specimens reached an average peak load of 11.5 kN after which they failed due to springline wall crushing. GFRP being a flexible and elastic material, the liners almost returned to the original shape and size after unloading.

The solid wall CFRP liners failed by wall crushing at the springline and delaminating at the crown simultaneously. There was a reversal of curvature at the crown, and the invert lifted and cracked. Since the CFRP is highly stiff, there was delamination between the laminate plies under high loads. A continuous crackling sound of individual fibers fracturing was observed until the specimens ultimately failed. This acoustic effect of the buckling fibers could have taken place as carbon fibers are brittle under loading. The CFRP liners ultimately failed by brittle fracture at springline. The cracks at springline started occurring at 7.5 kN and specimens reached a peak load of 13 kN. The reversal of curvature was recorded at an average load of 11 kN. CFRP specimens partially retained the reversed curvature at crown and lifted invert even after unloading. Figure 3-4 shows the modes of failure for CFRP liners and its deformed shape.

3.5.1.2 Sandwich Liners

The GFRP sandwich liners with 3-D woven fabric core showed the following modes of failure: core shear, overall buckling of the liners and skin delamination from core as presented in Figure 3-4. An audible springline crushing and visible cracking developed at an average load of 7.5 kN. An average peak load of 10.6 kN was attained by all the specimens. Skin buckling occurred in the direction away from the core and at the shoulders for the specimens 2G-W-2G - 2 and 2G-W-2G - 3. Interestingly, it was observed that the core shear was dominant at the shoulder and haunch positions of the liner. Based on previous studies, the diagonal tilting of vertical core fibers (core shear) occurs as the sandwich liners start behaving partially composite where the facesheets are stiff and the weak core is unable to maintain a linear strain profile due to a low rigidity. While bending, facesheets started behaving independently and the top and bottom facesheets start moving in directions opposite to each other creating shear stresses within the core. It ultimately compromised the stability of the system as the core shear deformation occurred.

CFRP sandwich specimens with 3-D woven fabric core had the same failure modes as that of GFRP specimens. Due to the high rigidity of carbon laminate, the facesheet delamination from the weak core occurred at a much lower load when compared to GFRP sandwich specimens. Springline cracking occurred at about 8 kN for all the specimens and the specimens reached an average peak load of 11.5 kN. Buckling near the plates was more prominent when compared to GFRP sandwiches, similar to solid wall CFRP specimens.

GFRP and CFRP sandwich specimens with bulkermat core failed due to core shear closer to the crown/invert positions and consequent delamination of the facesheet from the core was observed after failure. Core shear failure occurred as the maximum shear stress of the

core exceeded its ultimate shear stress. The GFRP and CFRP specimens reached an average peak load of 13.1 and 13.2 kN respectively, after which the core sheared and a sudden drop in load carrying capacity occurred.

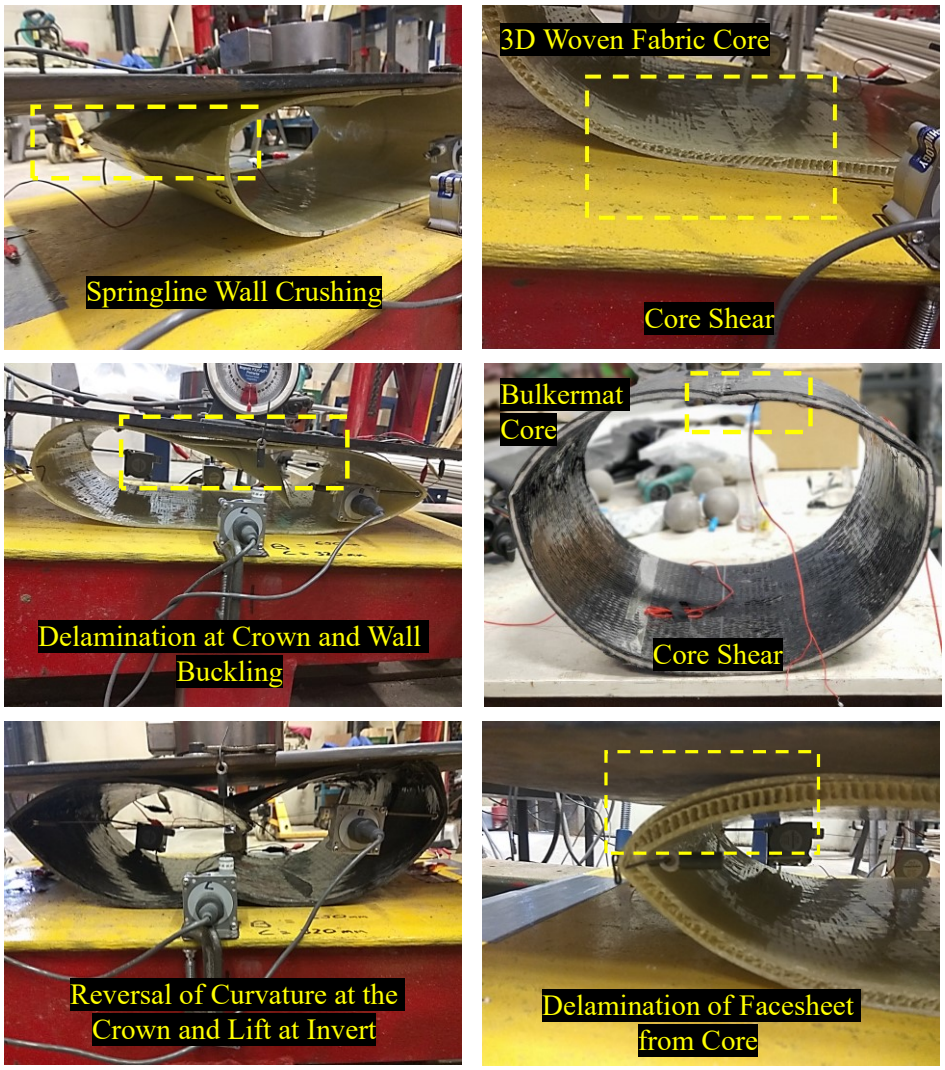

(a) **(b)**

Figure 3- 4 Modes of failure for (a) Solid Wall and (b) Sandwich Liners

Overall, the sandwich specimens had shown higher stiffness when compared to solid wall specimens. Especially, there is a significant difference of stiffness in the GFRP specimens of the both types. The sandwich specimens with 3-D core are stiffer but they have lower

strength than the solid wall specimens as they fail early due to core shear and further delamination. The sandwich specimens with bulkermat core though, has both higher strength and stiffness when compared to its counterparts. It was noticed that sandwich specimens with the 3-D woven fabric core when loaded under transverse compression, undergoes diagonal tilting of vertical core piles which are in the z-direction. Under compression load the focus is shifted to the bending resistance of the joints linking vertical fiber piles and the panel skins, from the geometric constraint on buckling. As the maximum shear stress in the core increases beyond the shear yield strength, the joints with bending-resistance starts resembling the function of plastic hinges. This weakens the structural integrity of the system, thereby lowering its ultimate strength.

3.5.2 Load – Diametrical Deflection Behavior

3.5.2.1 Solid Wall Liners

The results of load – diametrical deflection response for GFRP and CFRP liners based on the transverse compressive loading are given in Table 3-3 and their corresponding graphs are presented in Figure 3-5a. A total of four GFRP and two CFRP specimens were tested using two string potentiometers in each direction to measure the diametrical deflection. The average of the two were used for further calculations. However, the data from the two devices were very close to each other. Until an average load of 8 kN and 11 kN, the GFRP and CFRP specimens vary linearly, after which they start behaving non-linearly until they reach their peak load, based on Figure 3-5a.

As the load increases, the circular liner starts deforming elliptically thereby recording large levels deflection, which causes a non-linear load – diametrical deflection response in the

liner. This deformation is called elliptical ring deflection and it causes a non-linear behavior called geometric non-linearity in the FRP liners.

As expected, the CFRP specimens had a higher initial stiffness and peak load, hence showing minimum deflection when compared to GFRP specimens. An analytical model was developed to compare the vertical and horizontal deflection against the test data as the circular liner fails elliptically while loading under transverse compression, using Mathcad. The model is described in further sections of this report.

3.5.2.2 Sandwich Liners

Results of the load – diametrical deflection response of GFRP and CFRP sandwich liners with 3-D core based on the parallel plate load testing are given in Table 3-3 and their corresponding graphs in Figure 3-5c. A total of four GFRP and CFRP specimens respectively, were tested to find the deflection using string potentiometers. Based on Figure 3-5c, it is noticeable that until a load of 7 kN and 9.5 kN, the GFRP and CFRP specimens tend to behave linearly after which they become bi-linear/ non-linear. This non-linearity occurs as the core shears and starts behaving partially composite while deforming elliptically under loading. The specimen 2G-W-2G – 3 had two peaks when it was loaded to its maximum capacity where, after the first peak the overall buckling was dominant. In general, for both GFRP and CFRP specimens the core shear was the governing mode of failure.

Load – diametrical deflection behavior of GFRP and CFRP sandwich liners with bulkermat core is presented in Figure 3-5b. It can be observed that the relation between load and diametrical deflection is almost linear for sandwich specimens with this core material, until it reaches its ultimate load capacity. It also shows that this composite has higher initial

stiffness when compared to solid wall and 3-D core sandwich specimens. The elastic modulus of bulkermat is 6.6 times the elastic modulus of 3-D woven fabric core, because of which the bulkermat sandwich system has a high flexural rigidity.

Table 3- 3 Summary of Test Results based on Diametric Deflection

Specimen Type	Peak Load (kN)		Vertical Deflection at Peak Load (mm)		Horizontal Deflection at Peak Load (mm)	
	AVG	SD	AVG	SD	AVG	SD
4G	11.50	1.40	187.00	15.70	117.00	5.50
4C	13.00	0.12	63.50	27.80	42.80	13.90
2G-W-2G	10.60	0.93	194.00	44.90	119.50	22.80
2C-W-2C	11.50	0.61	152.00	30.50	90.90	14.80
2G-B-2G	13.07	1.54	59.00	54.00	37.00	29.00
2C-B-2C	13.15	1.64	18.00	12.00	12.00	6.00

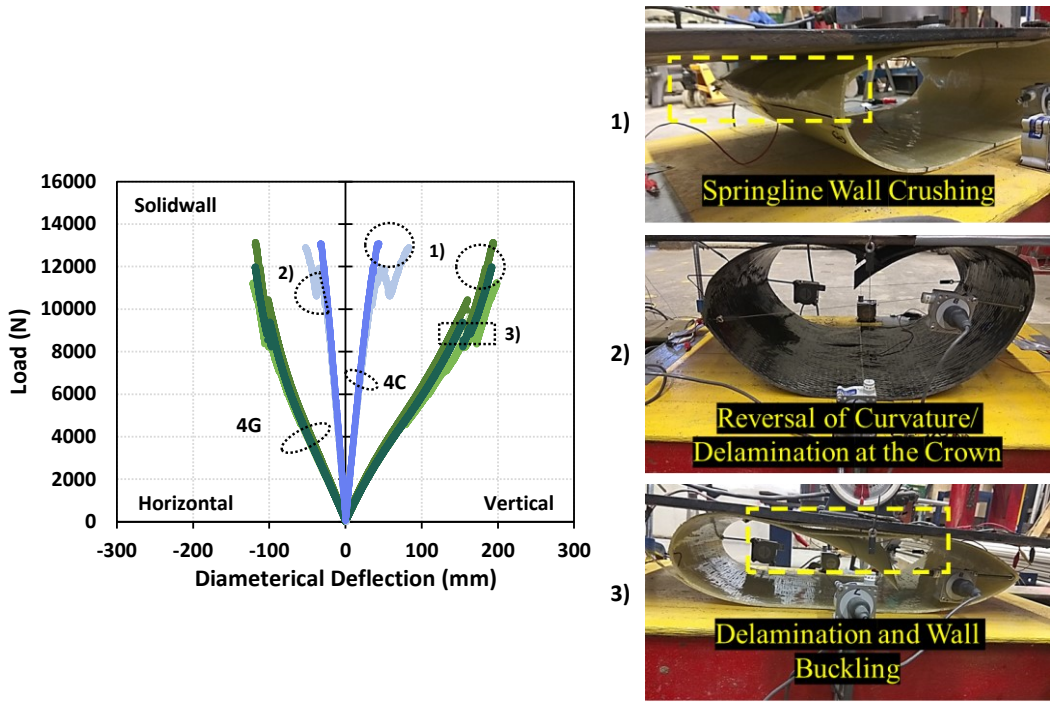

Figure 3- 5 (a) Load vs. Diametrical Deflection for Solid Wall Specimens

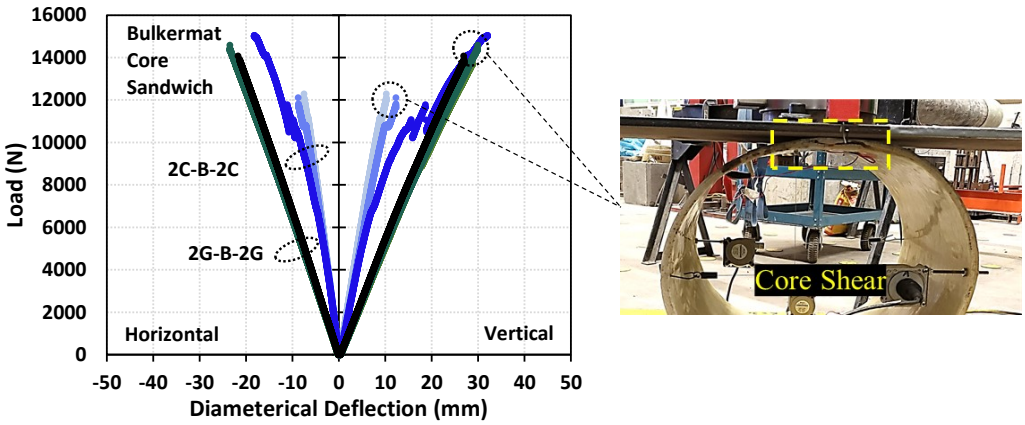

Figure 3- 6 (b) Load vs. Diametrical Deflection for Sandwich Specimens with Bulkermat Core

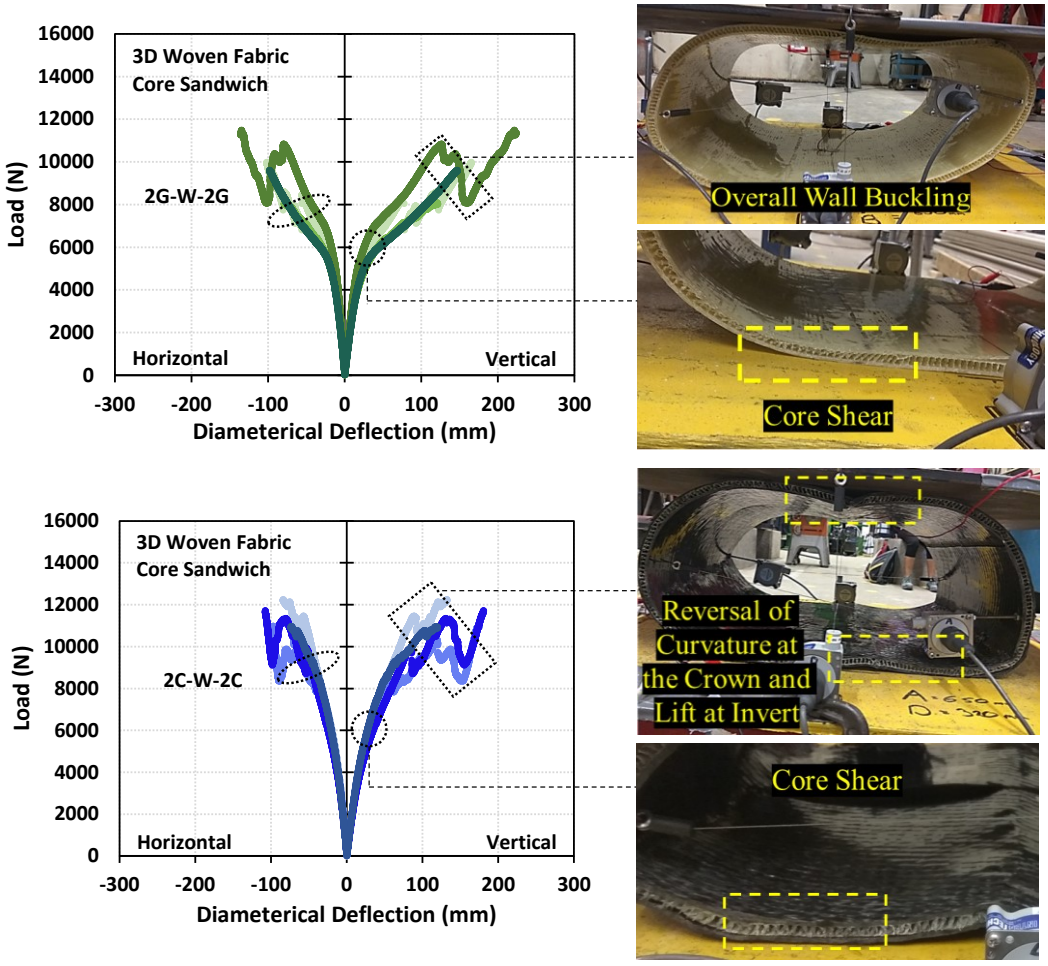

Figure 3- 7 (c) Load vs. Diametrical Deflection for Sandwich Specimens with 3-D Woven Fabric Core

3.5.3 Load – Strain Behavior

3.5.3.1 Solid Wall Liners

Strains at springline and crown/invert positions were collected using a DAQ with frequency of 10 Hz. Load – Strain behavior of GFRP and CFRP specimens at the springline and crown/invert positions are presented in Figure 3-6a. Due to the loss of some strain gauges during the test, the curves indicating load – strain response were continued based on their previous slope to the failure load. It is evident that CFRP a low ductility while comparing its load – strain graph against GFRP specimens.

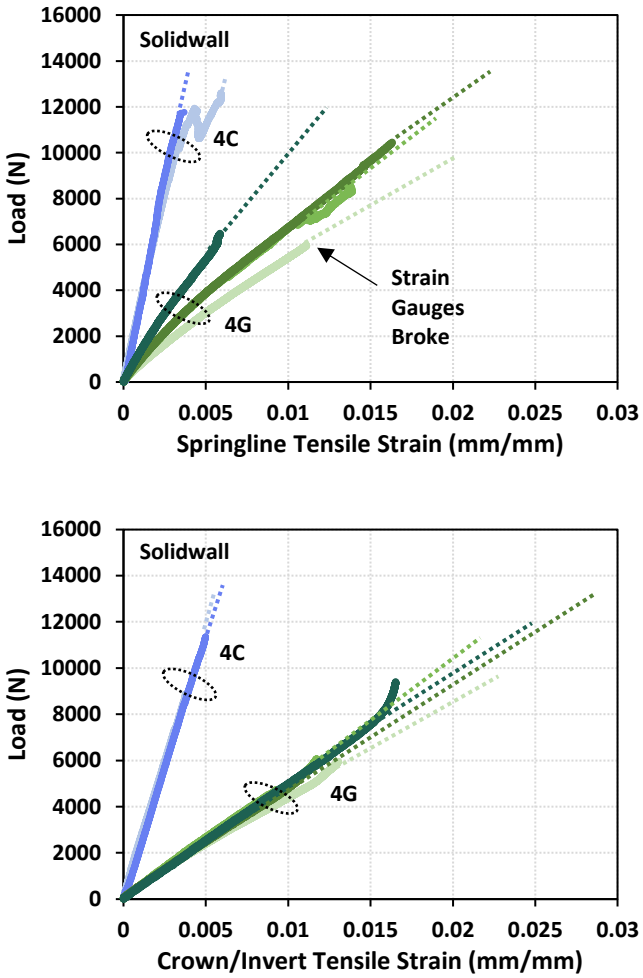

Figure 3- 8 (a) Load vs. Strain Behavior of FRP Specimens at Springline and Crown/Invert Positions for Solid Wall Specimens

CFRP specimens show less strain under their corresponding peak loads when compared to GFRP specimens accounting for the higher flexural stiffness in CFRP liners. The GFRP specimens showed less or no yielding and it is difficult to permanently deform this material under compressive loading. Since GFRP and CFRP specimens undergo maximum deflection in the vertical direction when compared to the horizontal direction, it is noticeable that the strain for a given load is higher at the crown/invert than the springline.

3.5.3.2 Sandwich Liners

Load - strain behavior of GFRP and CFRP sandwich liners with 3-D core are presented in Figures 3-6c based on strain data collected from the crown/invert and springline positions of the liner. The difference in strains for GFRP and CFRP sandwich liners at both springline and crown/invert positions are minimal. Like the solid wall specimens, the strain at crown/invert is higher when compared to springline substantiating for the higher vertical deflection when compared to the horizontal deflection. It can be noticed that the load strain graph for this sandwich specimens is mostly non-linear though it is a linear elastic material. It is because of the early onset of core shear and liner wall buckling.

Load – strain plots of GFRP and CFRP sandwich liners with bulkermat core are given in Figure 3-6b. It is noticeable that the load – strain behavior is linear at both springline and crown/invert positions. In comparison with the GFRP/CFRP 3-D woven fabric core specimens, the bulkermat sandwich specimens have a significantly low value of strain under their peak load - which again is higher than the other type of sandwich specimens in the crown/invert positions. This suggests that the change in vertical diameter of the bulkermat sandwich liners will be much lower than the 3-D woven core sandwich liners for a given load, which in turn would increase the PS of the bulkermat sandwich system.

Overall, these sandwich liners with bulkermat core have exhibited an almost full-composite behavior until failure unlike the composites with 3-D woven fabric core which behaved partially-composite, exhibiting a bi-linearity/ non-linearity in the system due to the early onset of core shear which caused a stiffness softening in the liners.

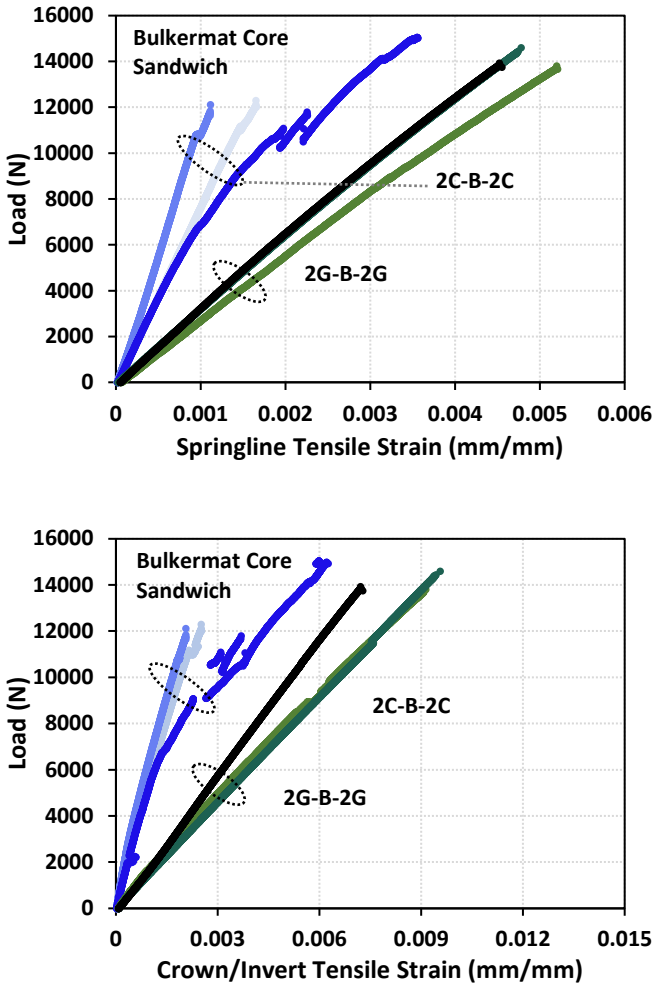

Figure 3- 9 (b) Load vs. Strain Behavior of FRP Specimens at Springline and Crown/Invert Positions for Sandwich Specimens with Bulkermat Core

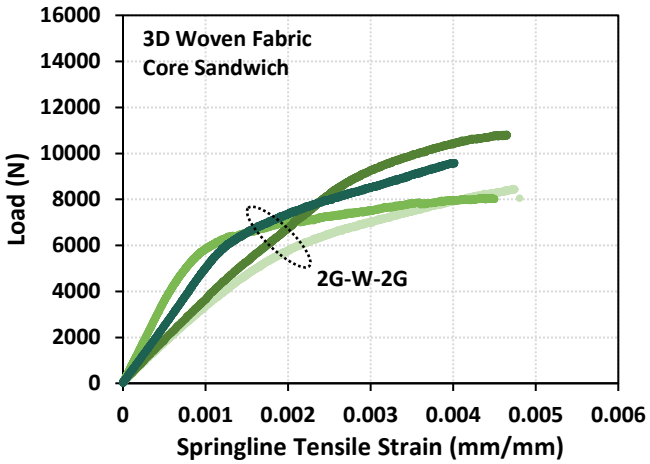
3D Woven Fabric
Core Sandwich
2G-W-2G
Load (N)
16000
14000
12000
10000
8000
6000
4000
2000
0
0
0.001
0.002
0.003
0.004
0.005
0.006
Springline Tensile Strain (mm/mm)

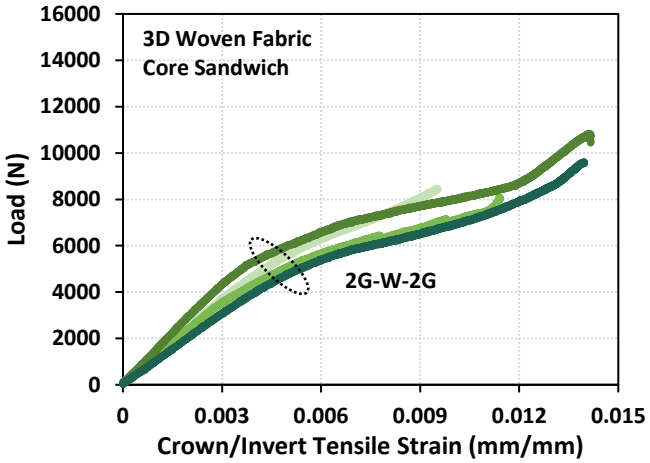
3D Woven Fabric
Core Sandwich
2G-W-2G
Load (N)
16000
14000
12000
10000
8000
6000
4000
2000
0
0
0.003
0.006
0.009
0.012
0.015
Crown/Invert Tensile Strain (mm/mm)

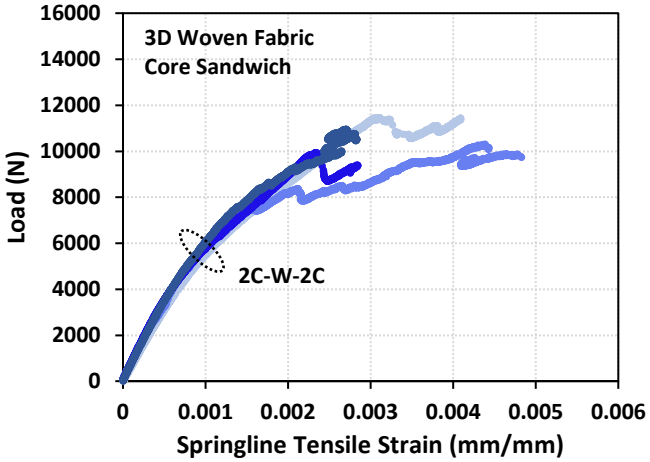
3D Woven Fabric
Core Sandwich
2C-W-2C
Load (N)
16000
14000
12000
10000
8000
6000
4000
2000
0
0
0.001
0.002
0.003
0.004
0.005
0.006
Springline Tensile Strain (mm/mm)

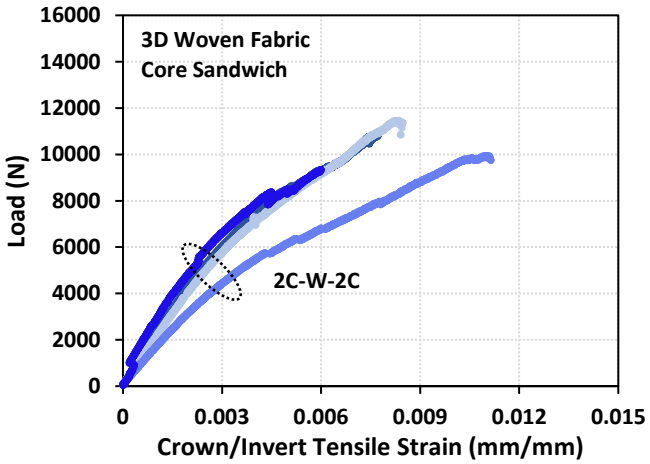

Figure 3- 10 (c) Load vs. Strain Behavior of FRP Specimens at Springline and Crown/Invert Positions for Sandwich Specimens with 3-D Woven Fabric Core

3.5.4 Pipe Stiffness and Stiffness Factor

The ratio of force per unit length of the specimen (F) to the deflection in pipe diameter (Δy) is called pipe stiffness (PS). It is also the slope of the load - deflection diagram. The pipe stiffness at 5% vertical deflection is used as the stiffness for design purposes in general.

$$PS = {}^{F}/_{\Delta y} \qquad (3\text{-}1)$$

The product of PS and the quantity 0.149 r^3, which is derived using mechanics relating to the total strain energy stored in a ring specimen is called as stiffness factor (SF).

$$SF = EI = PS \times (0.149\, r^3) \qquad (3\text{-}2)$$

where, E is the elastic modulus and I is the moment of inertia. In this study, the PS and SF for all the specimens were calculated at 1%, 2.5%, 5% and 10% vertical deflection and averaged as shown in Table 3-4. An $EI_{composite}$ was developed using cross-sectional analytics of the solid wall and sandwich sections. Since sandwich specimens are composite and made of different materials for facesheets and core respectively, its flexural stiffness

EI is the sum of the flexural stiffness of both facesheets and the core, measured about the centroidal axis of the cross-section,

$$EI_{sandwich} = E_c \frac{wc^3}{12} + E_f \frac{wt_f{}^3}{6} + E_f \frac{wt_f d^2}{2} \quad (3\text{-}3)$$

The cross-sectional details of a sandwich specimen are given in Figure 3-7. The $EI_{composite}$ for solid wall specimens is based on the results from tensile coupon test. Ply thickness of the coupon was used to find the normalized elastic modulus and the second moment of area was calculated based on the section properties. The model flexural rigidity was calculated per unit width. The EI based on test data was compared to the $EI_{composite}$ and the results are as shown in Table 3-4.

Based on the table it can be found that the 2C-B-2C has the highest SF and also has a higher ultimate strength comparatively. The ring stiffness of the 2G/C-W-2G/C were compromised as highly stiff facesheets were used with a weak core making the specimens behave partially composite.

3.6 SUMMARY

The formulation of the test matrix was briefly discussed in this chapter. The material properties determined by coupon tests were also reported. The specimen fabrication using a customized cardboard mandrel to make 3 or 4 liners at once was described. The test set up and instrumentation to find the elliptical ring deflection and PS of liners using the ASTM standards were discussed. The failure modes of solid wall and sandwich specimens were detailed. The load – deflection and load – strain behavior of the liners under transverse compression were studied and reported. The PS and SF were also found and recorded for all the six liner types.

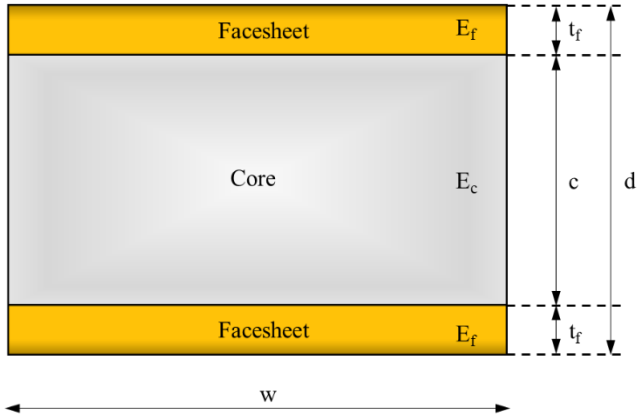

Figure 3- 11 Cross-section of a Sandwich Specimen

Table 3- 4 Summary of Test Results based on PS and EI

Specimen Type	PS at 1%*		PS at 2.5%*		PS at 5%*		PS at 10%*		EI at 1%*		EI at 2.5%*		EI at 5%*		EI at 10%*		EI Full Composite	Degree of Composite Action			
	AVG	SD	AVG	SD	AVG	SD	AVG	SD	AVG	SD	AVG	SD	AVG	SD	AVG	SD		at 1%	at 2.5%	at 5%	at 10%
4G	0.31	0.03	0.27	0.02	0.25	0.01	0.23	0.01	219	18	188	9	173	11	160	9	173	126	109	100	92
4C	1.21	0.04	1.18	0.02	1.14	0.04	1.03	0.06	902	33	878	8	849	24	766	41	1143	79	77	74	67
2G-W-2G	1.13	0.13	1.04	0.12	0.86	0.1	0.58	0.06	876	108	807	100	666	84	449	47	2265	39	36	29	20
2C-W-2C	0.97	0.03	0.91	0.05	0.79	0.06	0.61	0.05	752	17	705	33	614	33	474	27	12152	6	6	5	4
2G-B-2G	1.59	0.06	1.72	0.06	1.71	0.05	N.A	N.A	1133	49	1225	53	1216	43	N.A	N.A	1422	80	86	86	N.A
2C-B-2C	3.70	0.47	3.64	0.61	N.A	N.A	N.A	N.A	2618	334	2575	436	N.A	N.A	N.A	N.A	7160	37	36	N.A	N.A

Note: * 1%, 2.5%, 5% or 10% of vertical deflection (the unit of EI is kN-mm^2/mm and PS is MPa), NA: not available due to initial failure of specimens

CHAPTER 4 ANALYTICAL STUDIES

This chapter details about the analytical model that was developed using Mathcad to find the diametrical deflections and strains at springline and crown/invert positions by an iterative procedure. This section outlines the model description for both solid wall and sandwich FRP liners which behave geometrically non-linear due to large deformations under transverse compression. The model was verified against the experimental data and was used to conduct a parametric study. The effect of liner diameter, core thickness, facesheet thickness and shape geometry on the behavior of these liners have been studied and presented.

4.1 MODEL DESCRIPTION

Liners experienced large deformations while being loaded which caused a geometric non-linearity in the liner behavior. This analytics was focused on modelling geometric non-linearity, by finding subsequent horizontal and vertical deflections as the system became more elliptical. The corresponding strains at springline and crown/invert positions were found using the changing moments and longitudinal forces at the end of every iteration, which also helped in understanding the stress or geometric stiffening of the system. In sandwich composites the overall deflection is due to both bending and shear, unlike solid wall liners where the overall deflection is due to bending alone. Generally, the bending stresses are resisted by the facesheet and the shear is resisted by the core material in sandwich specimens. To accommodate this in the analysis, the strain energy in the sandwich system was taken to be the sum of strain energy due to bending and strain energy due to shear. The analysis procedure for both the major liner types are further discussed in this section.

4.1.1 Vertical and Horizontal Deflection

4.1.1.1 Solid Wall Liners

The liner was considered as a two-dimensional ring section, subjected to concentrated compressive forces along its vertical diameter. Due to symmetry, only a quadrant of the ring was considered for the analysis. Free body diagram of the elliptical ring with bending moments and the local constraints are shown in Figure 4-1. The magnitude of bending moment M_A in this cross section was statically indeterminate and was found using Castigliano's theorem. Since there was no rotation at point A while bending, displacement corresponding to M_A was zero.

$$dU/dM_A = 0 \tag{4-1}$$

where U is the strain energy of the quadrant of the ring. For any cross-section OX which is at an angle θ with the horizontal the bending moment is given as,

$$M_1 = M_A - F/2\ \rho \cos\theta \tag{4-2}$$

where, ρ is the radius of the curvature of the ellipse.

$$\rho = \frac{a \cdot b}{\sqrt{b^2\cos^2\theta + a^2\sin^2\theta}} \tag{4-3}$$

The decrease in vertical diameter was calculated based on Castigliano's theorem, using the total strain energy stored in the ring.

$$U = \frac{2}{EI}\int_0^{\pi/2} {M_1}^2 \rho\, d\theta \tag{4-4}$$

The vertical deflection δ_v was derived from the equation below:

$$\delta V = K_1 \left(F/EI\right) \tag{4-5}$$

where K_1 is an integral obtained by differentiating the strain energy U with respect to M_A as given below,

$$K_1 = \int_0^{\pi/2} \left(\rho \cos\theta - \frac{\int_0^{\pi/2} \rho^2 \cos\theta \, d\theta}{\int_0^{\pi/2} \rho \, d\theta} \right) \rho^2 \cos\theta \, d\theta \tag{4-6}$$

To determine the horizontal deflection δ_H, two equal and opposite imaginary forces Q were applied along the end of horizontal diameter. Calculating $\left({}^{dU}/_{dQ}\right)$ at Q = 0 would give the horizontal deflection. Figure 4-1 shows the free body diagram to find the increase in horizontal deflection. The moment M_2 and M_1 were summed up to find the δ_H as given below:

$$M_2 = M_B + {}^{Q}/_{2} \, \rho \sin\theta \tag{4-7}$$

$$\delta H = K_2 \left({}^{F}/_{EI}\right) \tag{4-8}$$

where K_2 is an integral obtained by differentiating the strain energy U with respect to M_B as given below,

$$K_2 = \int_0^{\pi/2} \left(\frac{\int_0^{\frac{\pi}{2}} \rho^2 \cos\theta \, d\theta}{\int_0^{\frac{\pi}{2}} \rho \, d\theta} - \rho \cos\theta \right) \left(\rho \sin\theta - \frac{\int_0^{\frac{\pi}{2}} \rho^2 \sin\theta \, d\theta}{\int_0^{\frac{\pi}{2}} \rho \, d\theta} \right) \rho \, d\theta \tag{4-9}$$

4.1.1.2 Sandwich Liners

For sandwich liners, the diametrical deflections were calculated based on the bending and shear capacities of the liners. To calculate the decrease in vertical diameter, the strain energy due to bending and strain energy due to shear were found. Strain energy due to bending was found as a function of load F.

$$U_b = 4. \int_0^{\pi/2} {M_1}^2 . \frac{\rho}{2. EI} d\theta \tag{4-10}$$

Strain energy due to shear was also found as a function of load F.

$$U_s = 4.\int_0^{\pi/2} V^2.\frac{\rho}{2.G.A}d\theta \tag{4-11}$$

where V is the shear force and G is the shear modulus. The overall strain energy was taken as the sum of strain energy due to bending and strain energy due to shear. The vertical deflection was obtained from the equation below.

$$\delta V_{\text{sandwich}} = {}^{dU}/_{dF} \tag{4-12}$$

Similarly, the horizontal deflection was found using the strain energy due to bending and strain energy due to shear as functions of the load F and imaginary forces Q. The horizontal deflection was determined using the equation below.

$$\delta H_{\text{sandwich}} = {}^{dU}/_{dQ} \tag{4-13}$$

4.1.2 Strain at Springline and Crown/Invert

For the analytical study, stress formula was used to determine the strain at springline and crown/invert positions of the liner.

$$\sigma = \frac{N}{A} \pm \frac{Mc}{I} \tag{4-14}$$

The longitudinal force N and shearing force V were determined as given below, using the free body diagram.

$$N = -\frac{F}{2}\sin\alpha \tag{4-15}$$

$$V = N\cot\alpha \tag{4-16}$$

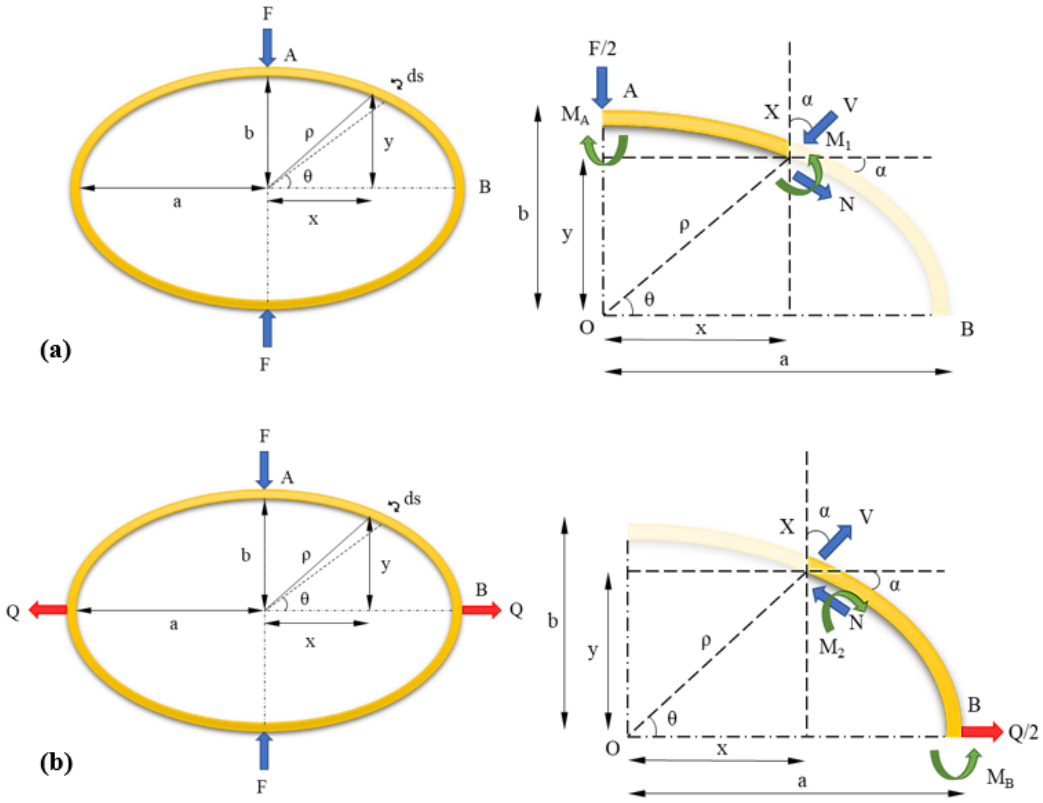

Figure 4- 1 Free Body Diagram of the Elliptical Ring to Calculate (a) Vertical and (b) Horizontal Deflection

4.2 Geometrical Nonlinearity

This analytical model was generated by considering the geometric nonlinearity that the liners exhibit while being loaded in transverse compression, through an iterative procedure. Under transverse compression, the circular liner starts failing elliptically with a decrease in vertical diameter and increase in horizontal diameter. The significant change of the geometric properties causes a large deformation which makes the load – diametrical deflection and load – strain behavior of the liner non-linear. As the liner geometry changes with the load, the normal force and moment capacity of the ring keep changing as well, causing a type of non-linearity in the system called geometric non-linearity. To mimic this ellipticity, a load of 500 N was added to the circular liner initially. δV and δH were

calculated under this load and added to the initial diameters respectively and a new radius of curvature was determined. Corresponding strains at springline and crown/invert positions were found simultaneously. For further iterations, the liner with the new radius of curvature were loaded with a force of 500 N consecutively, until the iterative data up to the desired load was obtained. Based on the data obtained from the iterations, load – diametrical deflection and load – strain curves were plot and compared against the experimental data. A flowchart discussing this process is presented as Figure 4-2.

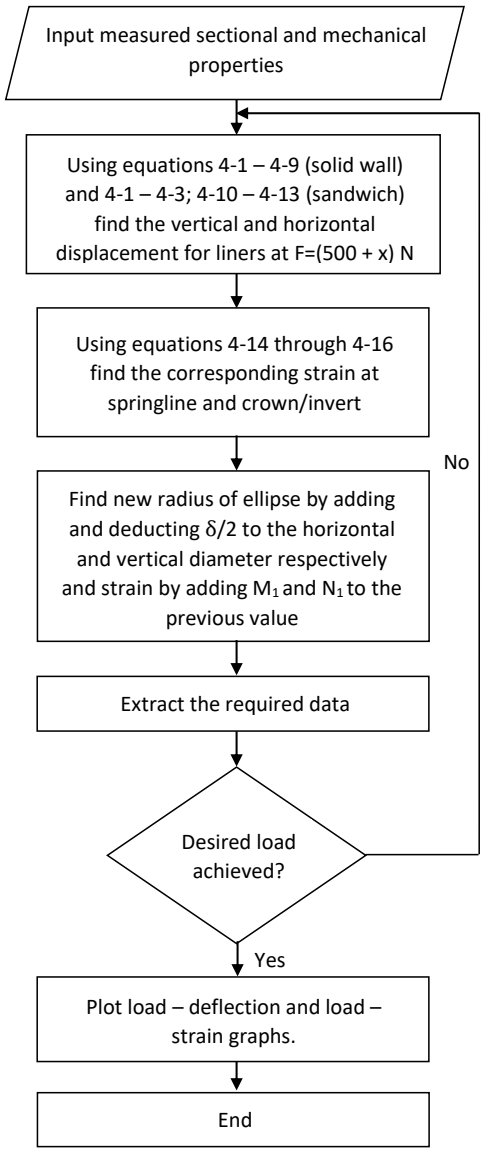

Figure 4- 2 Flowchart describing the Steps in Analytical Modelling

4.3 Model Verification

4.3.1 Solid Wall Liners

Figure 4-3 shows the verification of model against load – diametrical deflection behavior of GFRP and CFRP liners. From the figure it is evident that the model fits the data very well. GFRP having a low rigidity modulus when compared to CFRP deforms significantly under load and thereby shows large levels of deflections across the cross-section. These high levels of deflection in GFRP after an average load of 3kN causes a geometric non-linear behavior in the specimens. The model is able to capture the geometric non-linearity that the GFRP specimens display prominently while sufficiently accommodating for the mostly linear behavior that the CFRP specimens demonstrate as well. The model is able to validate that the GFRP specimens have a low stiffness until an average load of 9 kN and then starts gaining until it ultimately fails due to stress stiffening.

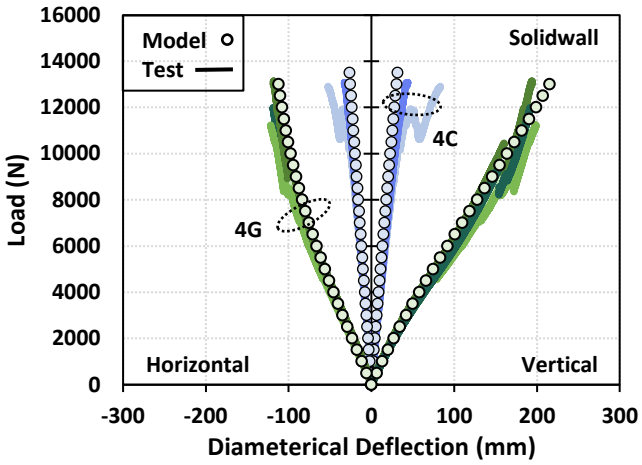

Figure 4- 3 Model Verification for Load- Diametrical Deflection Behavior of Solid Wall Liners

Figure 4-4 shows the load – strain behavior of GFRP and CFRP specimens in the springline and crown/invert positions, respectively. It must be noted that during the test some strain

gauges were lost. The curves have been continued up to the average peak load based on their previous slopes. The GFRP liners shows a conspicuous non-linear variation of strain with respect to load in both its springline and crown/invert positions while the CFRP liners remain almost linear. The strain was modelled using the results of changing thrust and moment at the end of every iteration. The model is able to capture the complete behavior of two different types of liner materials.

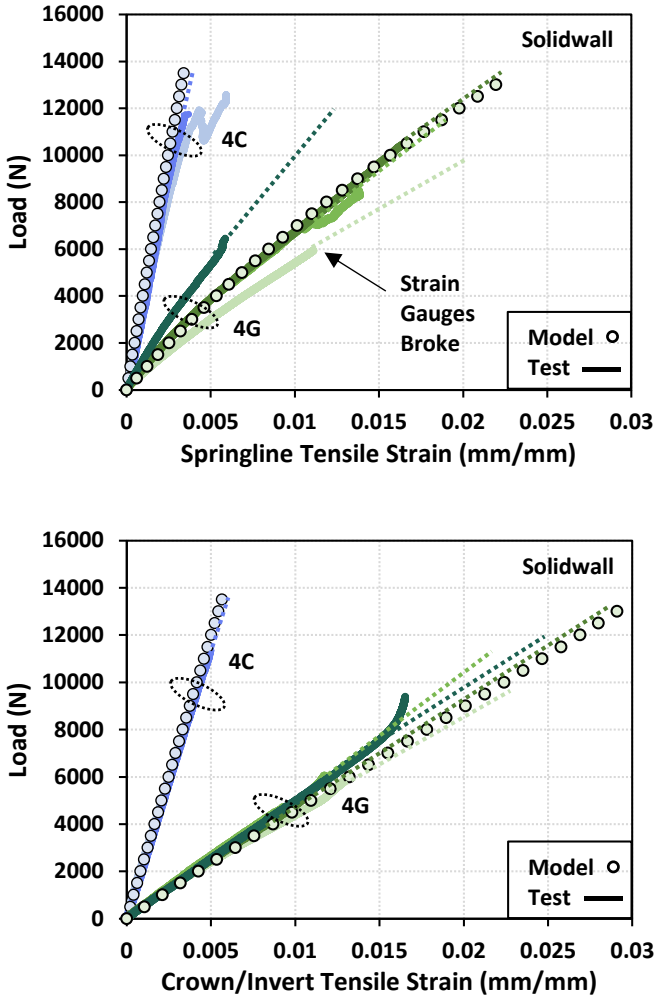

Figure 4- 4 Model Verification for Load- Strain Behavior of Solid Wall Liners at Springline and Crown/Invert Positions

4.3.2 Sandwich Liners

Figure 4-5 and 4-6 shows the model verification against the test results of load – deflection and load – strain behavior of GFRP and CFRP sandwich specimens with 3-D woven fabric core. A prominent discrepancy can be seen in the agreement between the model and test data in both the plots. This is due to the fact that, the model was developed to accommodate specimens with linear elastic material behavior which was fully composite until failure. However, the sandwich liners with 3-D woven fabric core displayed a partial-composite behavior after the early onset of core shear failure. The core shear modulus started reducing as the test proceeded and a bi-linearity/ non-linearity was developed in the system. It should be noted that the 3-D woven fabric core is a linear elastic material and hence material non-linearity was not considered in the analysis. This model was focused only on determining the deflections and strains of liners that had a full-composite behavior and modelling this bi-linearity/ non-linearity was out of the scope of this work.

Figure 4-7 and Figure 4-8 presents the load – deflection and load – strain behavior of GFRP and CFRP sandwich specimens with bulkermat core. It is evident that the model complies well with the test data. For the GFRP specimens the model is exactly the average of 3 curves whereas for the CFRP specimens, the stiffness is lower than the predicted model.

Overall, the model was also able to predict the failure mode of solid wall specimens as skin failure based on their rupture strain and as core shear for sandwich liner specimens based on their ultimate core shear strength. Also, model complied well for both the major liner types which were made of linear elastic materials until the load to which they behaved fully composite.

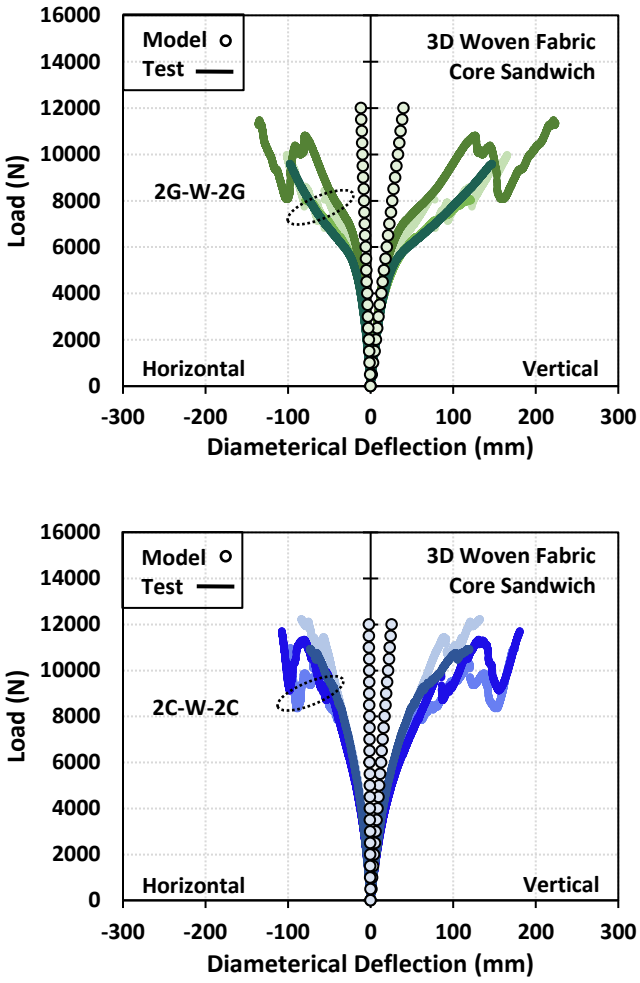

Figure 4- 5 Model Verification for Load- Diametrical Deflection Behavior of Sandwich Specimens with 3-D Woven Fabric Core

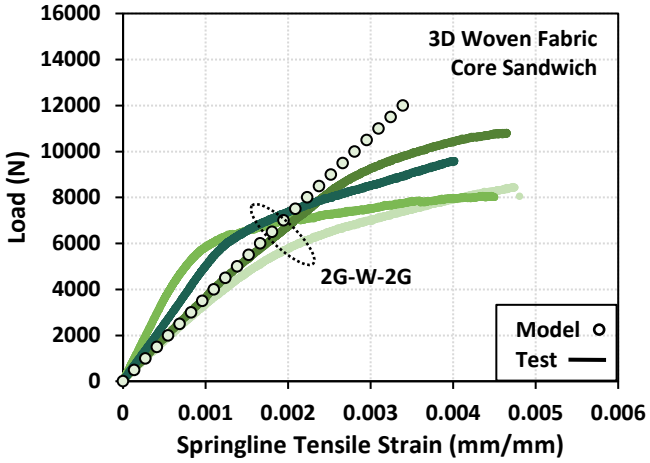

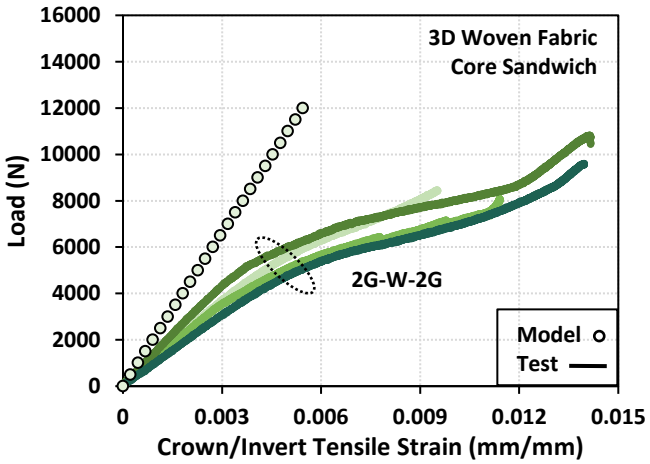

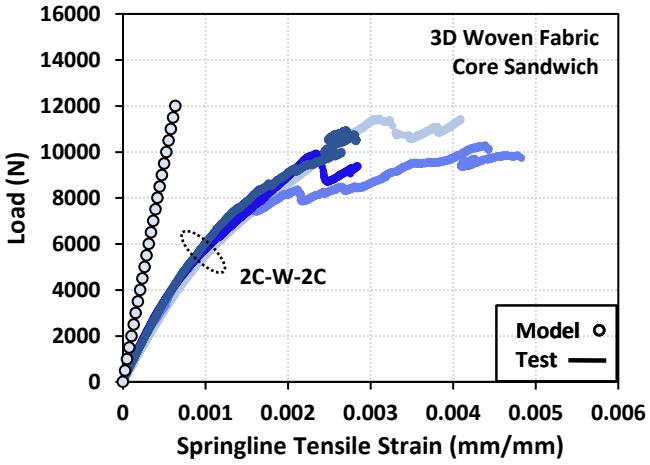

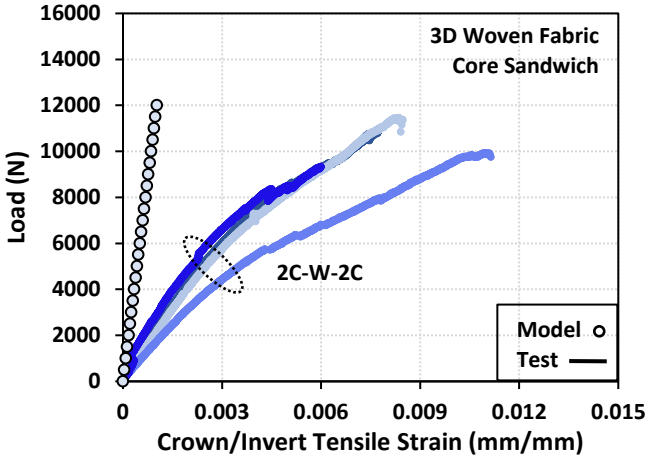

Figure 4- 6 Model Verification for Load- Strain Behavior of Sandwich Specimens with 3-D Woven Fabric Core at Springline and Crown/Invert Positions

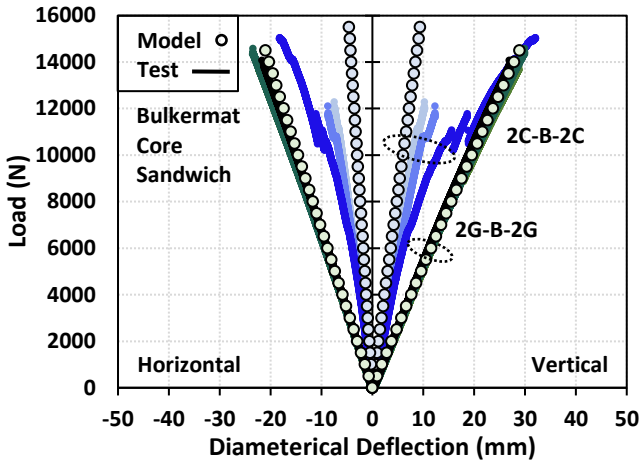

Figure 4- 7 Model Verification for Load- Diametrical Deflection Behavior of Sandwich Specimens with Bulkermat Core

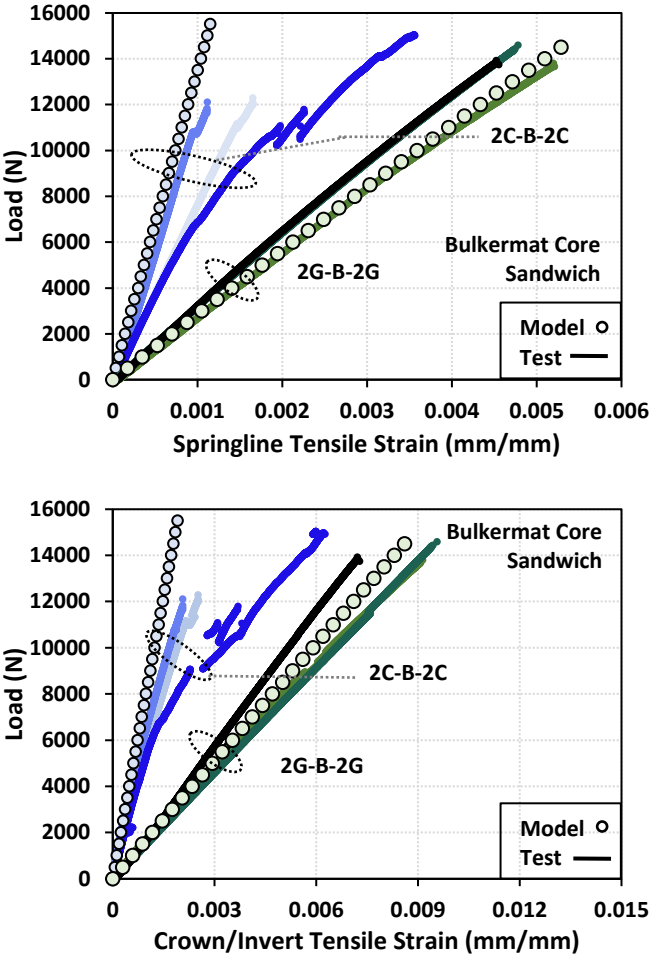

Figure 4- 8 Model Verification for Load- Strain Behavior of Sandwich Specimens with Bulkermat Core at Springline and Crown/Invert Positions

4.4 PARAMETRIC STUDY

A parametric study was conducted to study the effect of liner diameter, facesheet thickness, core thickness of the bulkermat sandwich liners and the shape geometry. The parameters that were kept constant while investigating the effect of the main parameter were W = 300 mm, $E_{f\ coupon,\ G}$ = 21,750 MPa, $E_{f\ coupon,\ C}$ = 100,000 MPa, $t_{f\ coupon,\ G}$ = 1.3 mm, $t_{f\ coupon,\ C}$ = 1.24 mm, E_c = 374.4 MPa and τ_{max} = 2.2 MPa. The results of this study are briefly reported in Table 4-1.

4.4.1 Effect of Liner Diameter

Four layer GFRP and CFRP solid wall liners with three diameter sizes, D = 300, 600 and 900 mm were considered for this study. Figure 4-3a and 4-3b shows the load – deflection and load – strain behavior of the 4G and 4C liners for the three cases. It is evident that the strength and stiffness of liners are dependent on the diameter. As the diameter increased, the stiffness and ultimate strength of the liner decreased. For example, on increasing the diameter from 300 to 900 mm, the strength of the liner reduced by 67.2% and 67.5% for the GFRP and CFRP liners, respectively. Also, Figure 4-3a and 4-3b shows that on increasing the diameter, geometric non-linearity became more prominent. Skin failure was the common failure mode. From Table 4-1, it is seen that with an increase in diameter, the stiffness of the liner decreased. However, the model overpredicts the failure of specimens in terms of strength.

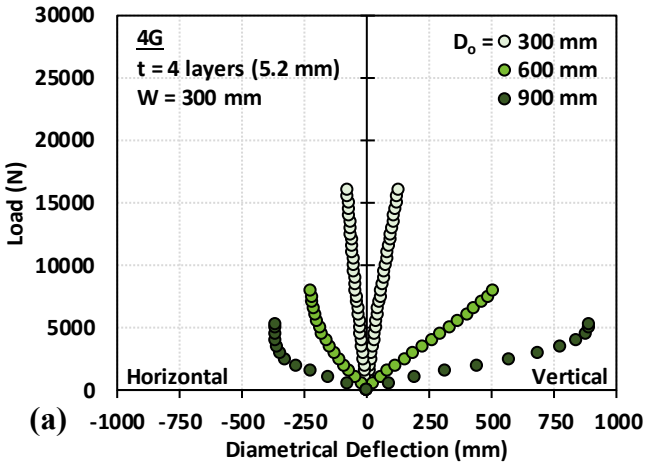
4G
t = 4 layers (5.2 mm)
W = 300 mm
D$_o$ = 300 mm
600 mm
900 mm
Horizontal
Vertical
Load (N)
30000
25000
20000
15000
10000
5000
0
-1000 -750 -500 -250 0 250 500 750 1000
Diametrical Deflection (mm)

(a)

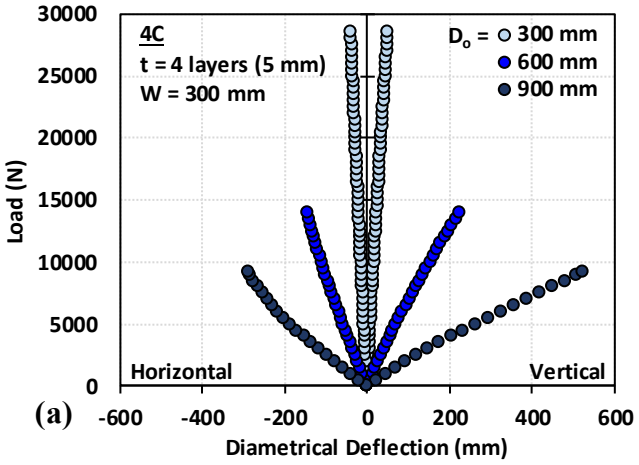
4C
t = 4 layers (5 mm)
W = 300 mm
D$_o$ = 300 mm
600 mm
900 mm
Horizontal
Vertical
Load (N)
30000
25000
20000
15000
10000
5000
0
-600 -400 -200 0 200 400 600
Diametrical Deflection (mm)

(a)

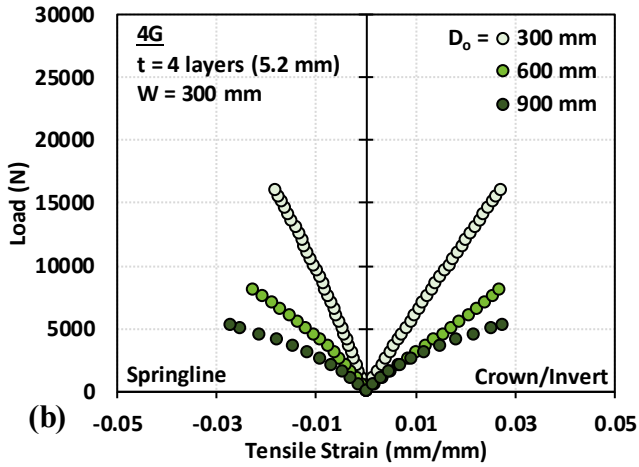
4G
t = 4 layers (5.2 mm)
W = 300 mm
D$_o$ = 300 mm
600 mm
900 mm
Springline
Crown/Invert
Load (N)
30000
25000
20000
15000
10000
5000
0
-0.05 -0.03 -0.01 0.01 0.03 0.05
Tensile Strain (mm/mm)

(b)

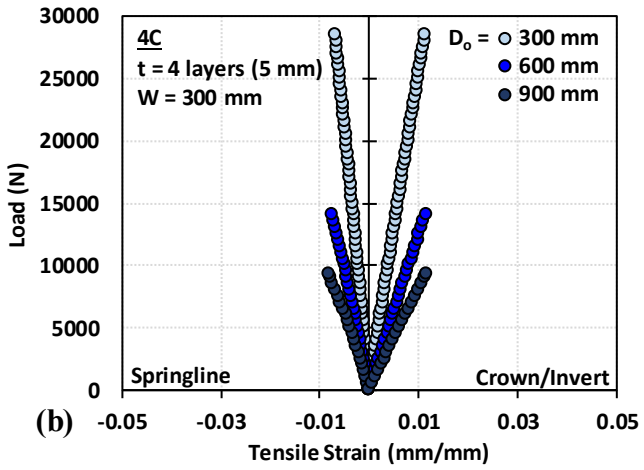

Figure 4- 9 (a) Load vs. Diametrical Deflection and (b) Load vs. Strain Behavior of Solid Wall Specimens based on Three Diameters

4.4.2 Effect of Core Thickness

The core thickness was varied as c = 0, 1, 2 and 3 layers with one layer being 4 mm thick for each 2G-nB-2G and 2C-nB-2C liners, where n is the number of layers. The ultimate strength and stiffness increased as the core thickness increased as seen in Figure 4-4. When the core thickness was increased from 0 to 3 layers, the strength increased by 66% for 2G-nB-2G liners. Based on Table 4-1, it was seen that the EI at 2.5%, 5% and 10% vertical deflection increased as the core thickness increased for both liner types. For example, there was an increase in stiffness by 95.72% at EI 2.5% when the core thickness was varied between 0 and 3 layers for 2G-nB-2G liners. Geometric non-linearity became less prominent with the increase in stiffness of the liners. Core shear was the governing failure mode for all liners. In certain cases, EI 5% and 10% vertical deflection was not available due to initial failure of the liner.

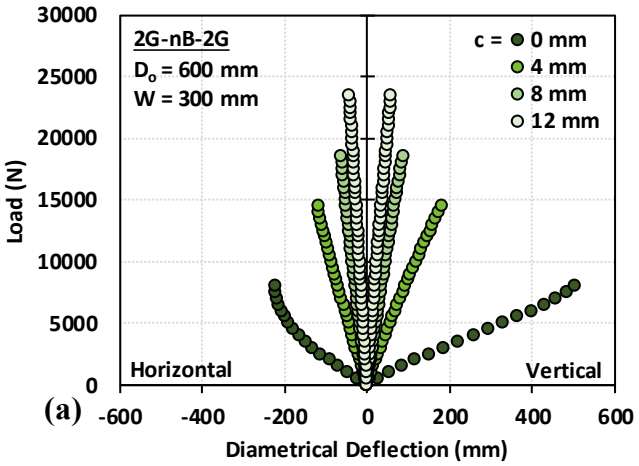
2G-nB-2G
D_o = 600 mm
W = 300 mm
c = 0 mm
4 mm
8 mm
12 mm
Horizontal
Vertical
Load (N)
Diametrical Deflection (mm)
30000
25000
20000
15000
10000
5000
0
-600
-400
-200
0
200
400
600

(a)

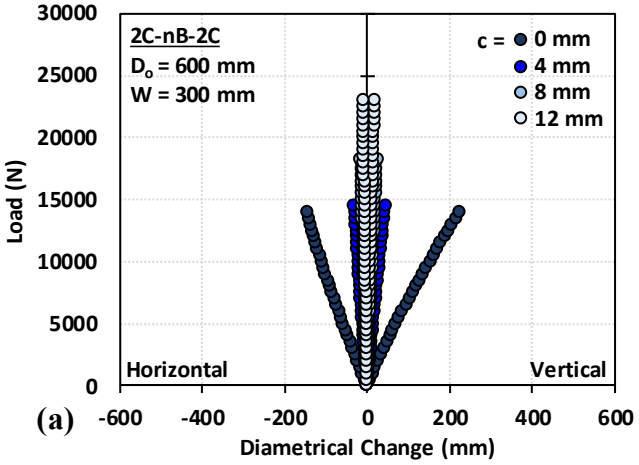
2C-nB-2C
D_o = 600 mm
W = 300 mm
c = 0 mm
4 mm
8 mm
12 mm
Horizontal
Vertical
Load (N)
Diametrical Change (mm)
30000
25000
20000
15000
10000
5000
0
-600
-400
-200
0
200
400
600

(a)

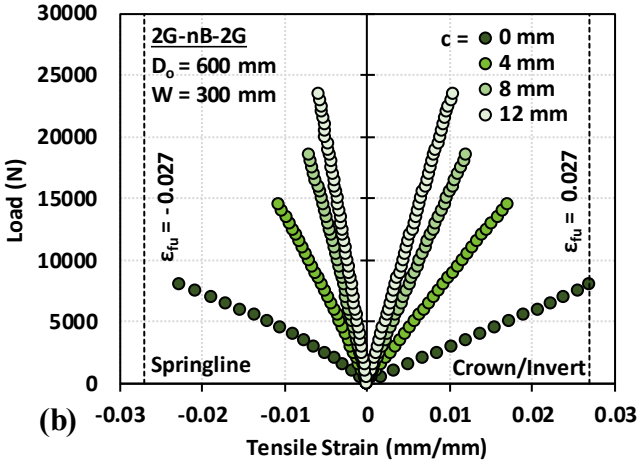
2G-nB-2G
D_o = 600 mm
W = 300 mm
c = 0 mm
4 mm
8 mm
12 mm
ε_{fu} = - 0.027
ε_{fu} = 0.027
Springline
Crown/Invert
Load (N)
Tensile Strain (mm/mm)
30000
25000
20000
15000
10000
5000
0
-0.03
-0.02
-0.01
0
0.01
0.02
0.03

(b)

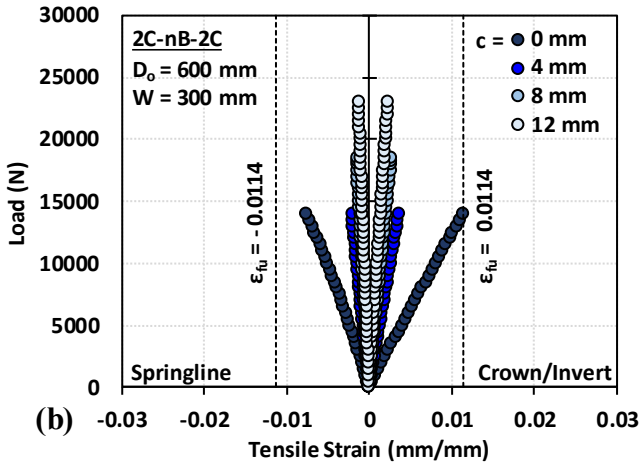

Figure 4- 10 (a) Load vs. Diametrical Deflection and (b) Load vs. Strain Behavior of Bulkermat Sandwich Specimens based on different Core Thicknesses

4.4.3 Effect of Facesheet Thickness

The facesheet thickness was varied between t_f = 1 to 3 layers with one layer being 1.3 mm and 1.24 mm thick for nG-B-nG and nC-B-nC liners, respectively. The strength and stiffness increased with an increase in facesheet thickness. The strength increased by 55% and 54 % for the nG-B-nG and nC-B-nC liners, respectively. Although there was an increase in stiffness, the geometric non-linearity of the liners was slightly observable for the nG-B-nG type. From table 4-1, it was noticeable that the stiffness factor increased as the facesheet thickness increased. The failure mode for all the specimens were core shear. The load – diametrical and load- strain plots based on the effect of changing facesheet thickness is given in Figure 4-5.

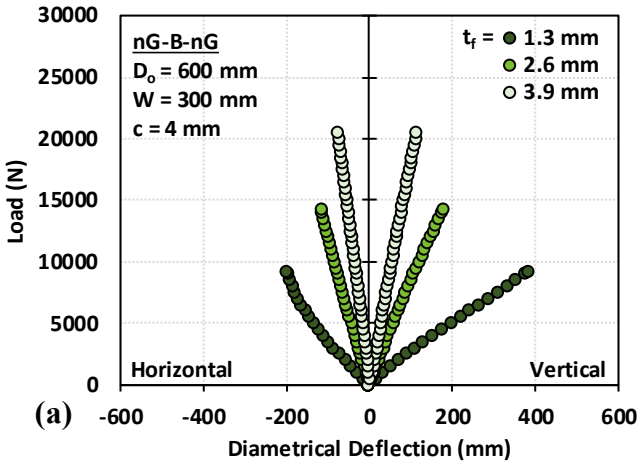
nG-B-nG
D_o = 600 mm
W = 300 mm
c = 4 mm
t_f = 1.3 mm
2.6 mm
3.9 mm
Horizontal
Vertical
Load (N)
Diametrical Deflection (mm)
30000
25000
20000
15000
10000
5000
0
-600
-400
-200
0
200
400
600

(a)

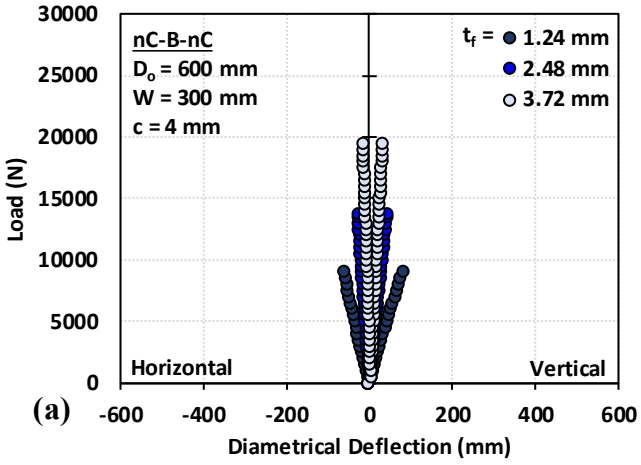
nC-B-nC
D_o = 600 mm
W = 300 mm
c = 4 mm
t_f = 1.24 mm
2.48 mm
3.72 mm
Horizontal
Vertical
Load (N)
Diametrical Deflection (mm)
30000
25000
20000
15000
10000
5000
0
-600
-400
-200
0
200
400
600

(a)

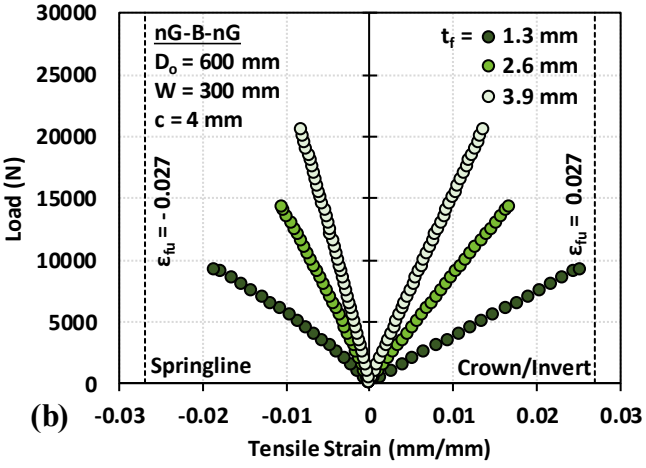
nG-B-nG
D_o = 600 mm
W = 300 mm
c = 4 mm
t_f = 1.3 mm
2.6 mm
3.9 mm
ε_{fu} = - 0.027
ε_{fu} = 0.027
Springline
Crown/Invert
Load (N)
Tensile Strain (mm/mm)
30000
25000
20000
15000
10000
5000
0
-0.03
-0.02
-0.01
0
0.01
0.02
0.03

(b)

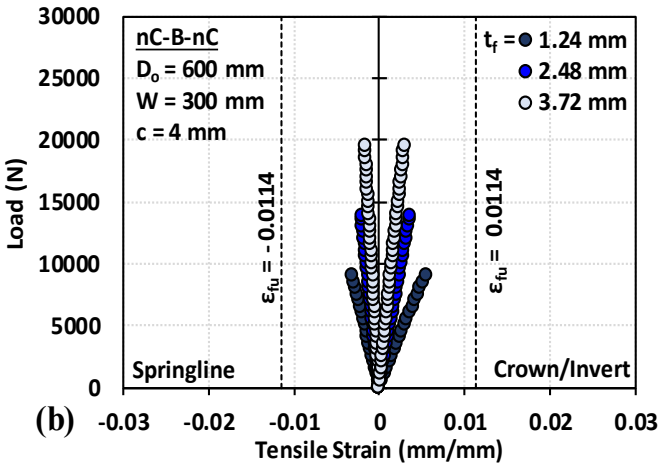

Figure 4- 11 (a) Load vs. Diametrical Deflection and (b) Load vs. Strain Behavior of Bulkermat Sandwich Specimens based on Changing Facesheet Thickness

4.4.4 Effect of Shape Geometry

The liner shape was varied from a circle to a horizontal ellipse with the following dimensions: 2a = 2b = 600 mm, 2a = 600 mm / 2b = 450 mm and 2a = 600 mm / 2b = 300 mm. The effect of shape geometry was studied for 4G, 4C, 2G-B-2G and 2C-B-2C liner types for all the 3 shapes. The 4G and 4C liners had a significant increase in strength and stiffness, whereas the 2G-B-2G and 2C-B-2C liners only stiffened with no change in strength as the vertical diameter decreased (more elliptical). Figure 4-6 shows the increase in stiffness of the liners as the vertical diameter decreased, but table 4-1 shows a decrease in stiffness with changing diameter. This is because, the EI in table 4-1 is calculated per 300 mm width. Also, the cross-sectional area of ellipse was lower than a circle with the same perimeter. Under loading, the ellipse offers enough resistance to approach a circular state, thereby achieving a greater strength and stiffness.

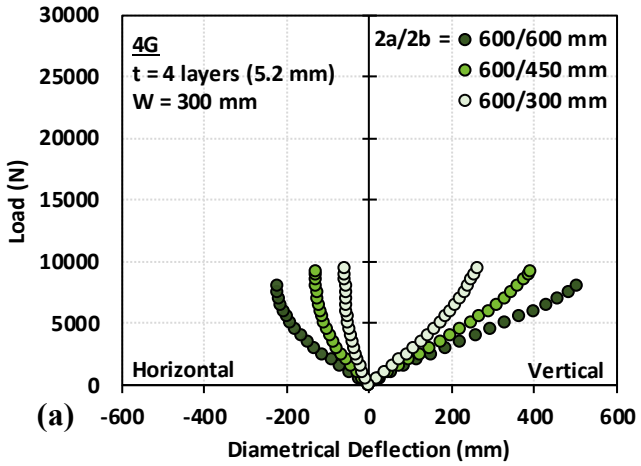
4G
t = 4 layers (5.2 mm)
W = 300 mm
2a/2b = 600/600 mm
600/450 mm
600/300 mm
Horizontal
Vertical
Load (N)
30000
25000
20000
15000
10000
5000
0
-600
-400
-200
0
200
400
600
Diametrical Deflection (mm)

(a)

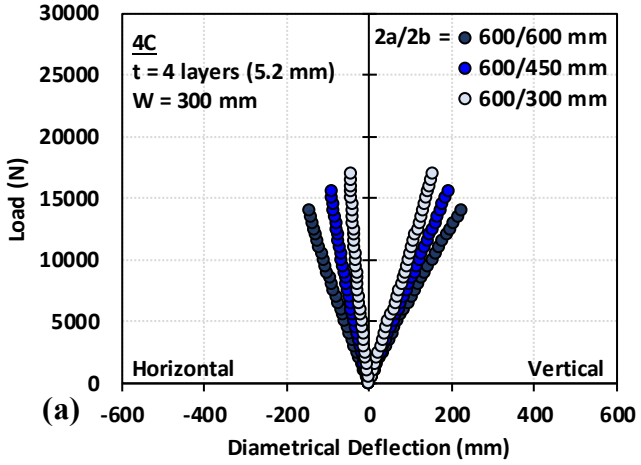
4C
t = 4 layers (5.2 mm)
W = 300 mm
2a/2b = 600/600 mm
600/450 mm
600/300 mm
Horizontal
Vertical
Load (N)
30000
25000
20000
15000
10000
5000
0
-600
-400
-200
0
200
400
600
Diametrical Deflection (mm)

(a)

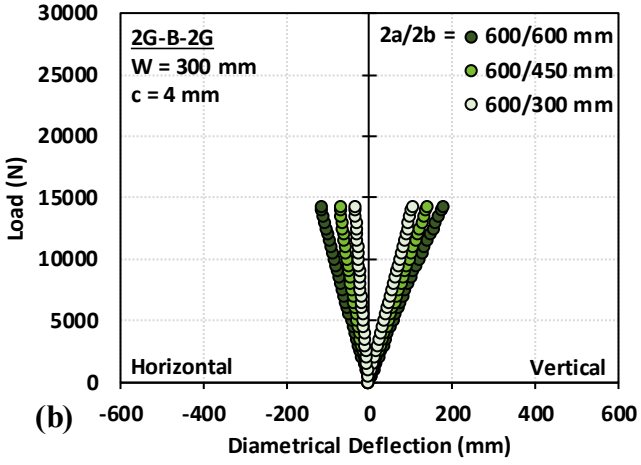
2G-B-2G
W = 300 mm
c = 4 mm
2a/2b = 600/600 mm
600/450 mm
600/300 mm
Horizontal
Vertical
Load (N)
30000
25000
20000
15000
10000
5000
0
-600
-400
-200
0
200
400
600
Diametrical Deflection (mm)

(b)

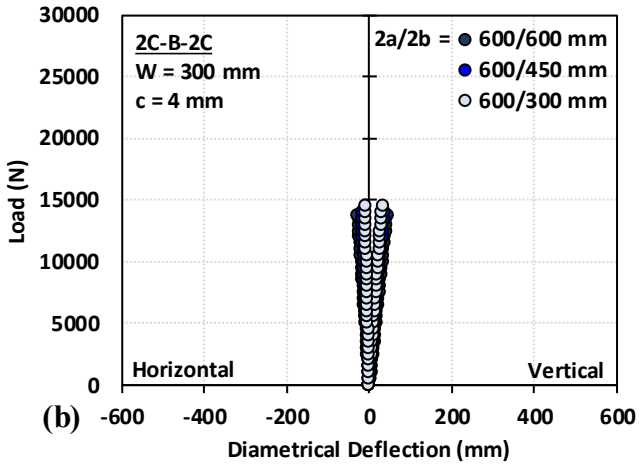

Figure 4- 12 Load vs. Diametrical Deflection Behavior of (a) Solid Wall (b) Bulkermat Sandwich Specimens based on Changing Shape Geometry

4.5 SUMMARY

The model description to find the vertical and horizontal deflections, and the strain at springline and crown/invert positions were detailed in this section. A flowchart depicting the consideration of geometric non-linearity for this analysis was also given. The model verification against the test data and the limitations of the model were also briefed. A parametric study was conducted using this model to study the effect of various parameters on the liner behavior.

Table 4- 1 Summary of Parametric Study

Case #	Skin Type	D_o (mm)	c (mm)	Number of Skin Layers	EI 2.5%	EI 5%	EI 10%	Peak load (kN)	Vertical Def. at Peak Load (mm)	Mode of Failure
1	Glass	300	0	4	251	246	236	16.00	126.23	Skin Failure
2	Carbon	300	0	4	999	975	937	28.50	50.98	Skin Failure
3	Glass	600	0	4	255	221	242	8.00	505.03	Skin Failure
4	Glass	600	4	2	1219	1194	1150	14.50	180.28	Core Shear
5	Glass	600	8	2	2916	2861	2763	18.50	86.62	Core Shear
6	Glass	600	12	2	5262	5167	5002	23.50	57.81	Core Shear
7	Carbon	600	0	4	1004	981	943	14.00	224.39	Skin Failure
8	Carbon	600	4	2	4416	4344	N.A	14.50	43.45	Core Shear
9	Carbon	600	8	2	9594	N.A	N.A	18.25	24.12	Core Shear
10	Carbon	600	12	2	15784	N.A	N.A	23.00	17.98	Core Shear
11	Glass	600	4	1	398	389	374	9.25	386.46	Core Shear
12	Glass	600	4	2	1005	1091	1102	14.25	179.38	Core Shear
13	Glass	600	4	3	1683	2115	2263	20.50	115.76	Core Shear
14	Carbon	600	4	1	1549	1520	1467	9.00	81.56	Core Shear
15	Carbon	600	4	2	3676	3986	N.A	13.75	43.58	Core Shear
16	Carbon	600	4	3	5806	7217	N.A	19.50	33.41	Core Shear
17	Glass	2a = 600 2b = 450	0	4	120	120	174	9.25	392.08	Skin Failure
18	Carbon	2a = 600 2b = 450	0	4	478	474	466	15.50	191.61	Skin Failure
19	Glass	2a = 600 2b = 450	1	2	573	568	560	14.25	140.84	Core Shear
20	Carbon	2a = 600 2b = 450	1	2	2031	1969	N.A	14.00	37.23	Core Shear
21	Glass	2a = 600 2b = 300	0	4	43	43	57	9.50	261.01	Skin Failure
22	Carbon	2a = 600 2b = 300	0	4	170	170	171	17.00	152.64	Skin Failure
23	Glass	2a = 600 2b = 300	1	2	200	120	200	14.25	105.10	Core Shear
24	Carbon	2a = 600 2b = 300	1	2	691	692	695	14.00	30.81	Core Shear
25	Glass	900	0	4	255	255	254	5.25	891.21	Skin Failure
26	Carbon	900	0	4	1018	994	952	9.25	523.23	Skin Failure

Note: * 1%, 2.5%, 5% or 10% of vertical deflection (the unit of EI is kN-mm^2/mm)

CHAPTER 5 CONCLUSION AND RECOMMENDATIONS

The focus of this research was to understand the actual behavior and structural capabilities of solid wall and sandwich FRP liners under transverse compression to use them as structural liners for deteriorated buried pipes. It was important to analyze and understand the effect of geometric non-linearity displayed by the liners as they largely deformed under loading. Also, establishing a data platform to develop a reliable design methodology for the rehabilitation of buried pipes using FRP liners was critical, considering the alarming rate of increase in deteriorated pipes by the day. To achieve these motives, the performance of GFRP and CFRP solid wall liners and sandwich liners with either 3-D woven fabric core or bulkermat core under transverse compressive loading were studied. A custom-made parallel plate test machine was set up, to measure the vertical and horizontal diametrical deflection and tensile strain at springline and crown/invert position as the liner deformed. An analytical model through an iterative procedure was developed to find the elliptical ring deflections and their corresponding tensile strains at springline and crown/invert using Mathcad. A parametric study was also conducted using the model to analyze the effect of liner diameter, core thickness, facesheet thickness and shape geometry, and the results were briefly discussed.

Based on the experimental and analytical studies, the following conclusions were drawn:

- The solid wall liners failed due to crushing of springline, whereas the governing mode of failure for sandwich liners was core shear. There was a significant difference in the failure of the two sandwich specimens as the specimens with 3-D woven fabric core showed a partial composite behavior as it was being loaded, such that the facesheets and core started behaving independently. In this study, two

layers of facesheets and one layer of the spacer was used. The high stiffness of facesheets compromised the structural performance of this system. Hence it is recommended, to not use more than one layer of facesheet for this sandwich type.

- An important element of this research was to determine and increase the ring stiffness of solid wall liners to create more sustainable and economic solutions for the structural rehabilitation of buried pipes. This was achieved by introducing two different spacer fabrics which increased the moment of inertia across the cross section. It was found that the CFRP bulkermat sandwich specimens had the highest PS and EI at 2.5% vertical deflection. However, the specimen failed before it reached 5% deflection and showed only 36% composite behavior at 2.5%.
- Bulkermat sandwich specimens had higher strength and ring stiffness with the same number of facesheets as that of solid wall and 3-D woven fabric core sandwich specimens as given Table 3-3 and Table 3-4.
    - There was a 14% and 1.5% increase in strength when bulkermat was introduced as a spacer in solid wall GFRP and CFRP specimens, respectively. Bulkermat was stronger by 24% and 15% when compared to its GFRP and CFRP 3-D woven core sandwich liner counterparts, respectively.
    - The stiffness of solid wall liners were increased by 6.3 times for GFRP and 3.1 times for CFRP specimens when bulkermat was introduced. Similarly, GFRP bulkermat sandwich specimens were 1.65 times stiffer and CFRP bulkermat specimens were 4 times stiffer when compared to its 3-D woven fabric sandwich counterparts at 2.5% vertical diametrical deflection.
- The analytical model was in good accordance with the test results for specimens

with linear elastic material which behaved fully composite until failure. It could encompass the concept of elliptical ring failure and could account for the geometric non-linearity caused due to large deformations in liner cross-section. However, the 3-D woven fabric core sandwich specimens behaved partially composite after the core shear. The model could not able to capture its bi-linear/ non-linear behavior.

- Based on the parametric study, it can be concluded that increasing the core thickness by one layer increased the EI by 2 times, whereas increasing one layer of facesheet increases the EI by 1.5 times. Increasing the core thickness also increased the ultimate strength of the specimens.

The following are recommended to expand the research further:

- It is important to conduct an in place evaluation of long-term ring stiffness of buried pipes and study the effect of aggressive soil conditions, burial depth, compaction of backfill on the stiffness and strength of the liner.
- Liners of different fiber-resin-core combinations have to be found and tested, which can increase the ring stiffness, load carrying capacity and durability of the pipes.
- Studies on feasibility and behavior of various hybrid sandwich system, to create more economic and sustainable solutions has to be conducted.
- The analytical model can be improved to account for partial composite behavior of liners, non-linear elastic material behavior and interface shear. The effect of soil confinement could be an added feature to this analysis.
- Study of behavior of these liners under both static and dynamic loads for various specimen sizes will help understand their mechanical performance and be useful for design purposes.

BIBLIOGRAPHY

Abraham, D.M. and Gillani, S.A. (1999). Innovations in materials for sewer system rehabilitation. *Tunnelling and Underground Space Technology*. 14(1):43-56.

Allen H.G. (2013). Analysis and design of structural sandwich panels. Pergamon Press, Oxford, UK.

Arjomandi, K. and Taheri, F. (2010). Elastic Buckling Capacity of Bonded and Unbonded Sandwich Pipes Under External Hydrostatic Pressure. *Journal of Mechanics of Materials and Structures*. 5(3):391-408.

Arjomandi, K. and Taheri, F. (2011). A new look at the external pressure capacity of sandwich pipes. *Marine Structures*. 24(1):23-42.

Arjomandi, K. and Taheri, F. (2012). Bending capacity of sandwich pipes. *Ocean Engineering*. 48:17-31.

ASTM D3039. (2017). Standard Test Method for Tensile Properties of Polymer Matrix Composite Materials. ASTM International, West Conshohocken, PA, USA.

ASTM. D2412. (2018). Standard Test Method for Determination of External Loading Characteristics of Plastic Pipe by Parallel-Plate Loading. ASTM International, West Conshohocken, PA, USA.

Aylor Jr., H.H. and Hirtz, B.A. (1990). Method of reconstructing pipe systems using fiberglass laminates. *U.S. Patent No. 4,897,135*.

Ballinger, C.A. and Drake P.G. (1995). Culvert Repair Practices Manual, Vol. 1, Report FHWA-RD-94-096. *Federal Highway Administration*, McLean, Va. 1:265.

Betts, D., Sadeghian, P. and Fam, A. (2018). Experimental Behavior and Design-Oriented Analysis of Sandwich Beams with Bio-Based Composite Facings and Foam Cores. *Journal of Composites for Construction*. 22(4).

Bhattachar, D.V. (2007). Development of an Asset Management Model for Culvert Inventory and Inspection. MASc Thesis. School of Planning, Design and Construction. Michigan State University, Michigan, USA.

Campaner, P., D'Amico D., Ferri, P., Longo, L., Maffezzoli, A., Stifani, C., Tarzia, A., Franz S., and Frank, W. (2010). Cardanol Based Matrix for Jute Reinforced Pipes. *Macromolecular Symposia*. 296(1): 526-30.

Corey, R. (2015). Protection of Buried Flexible Pipes with a Geosynthetic: Experimental and Numerical Studies. Ph.D. Dissertation. Faculty of Civil, Environmental, and Architectural Engineering. University of Kansas, USA.

Das, R.R. and Baishya, N. (2016). Failure Analysis of Bonded Composite Pipe Joints Subjected to Internal Pressure and Axial Loading. *Procedia Engineering*. 144:1047-1054.

Deniz, M.E., Ozen, M., Ozdemir, O., Karakuzu, R., and Icten, B. M. (2013). Environmental effect on fatigue life of glass–epoxy composite pipes subjected to impact loading. *Composites: Part B*. 44(1):304-312

Ehsani, M. (2012). Introducing a New Honeycomb-FRP Pipe. *In Pipelines 2012: Innovations in Design, Construction, Operations, and Maintenance, Doing More with Less*. 1084-1091.

Ehsani, M. (2019). A New FRP Solution for Reconstruction of Deteriorated Pipes and Culverts. *37th International No-Dig Conference and Exhibition*. Ref #2328

Ehsani, M. (2019). FRP 101:Taking the Mystery Out of Trenchless Repair of Pressure Pipes with Carbon FRP. *37th International No-Dig Conference and Exhibition*. Ref #2329

Garcíaa, D.B. and Moore, I.D. (2015) Performance of deteriorated corrugated steel culverts rehabilitated with sprayed-on cementitious liners subjected to surface loads. *Tunnelling and Underground Space Technology*. 47:222-232.

Geraghty, M., Pridmore, A., & Sanchez, J. (2011). Transitioning from leak detection to leak prevention: proactive repair of steel pipelines using fiber reinforced polymer (FRP) composites. *In Pipelines 2011: A Sound Conduit for Sharing Solutions*. 100-107.

Hansen U. (1998). Compression Behavior of FRP Sandwich Specimens with Interface Debonds. *Journal of composite materials*. 32(4):335-360.

Houssam, T. and Sean, D. (2001). Stress modeling of pipelines strengthened with advanced composites materials. *Thin-Walled Structures*. 39(2):153-165.

Imoto, T., Seshimo, M., Makimoto, F. and Kitagawa, E., Ashimori Industry Co Ltd. (1993). Lining material for pipelines and a process for providing pipelines therewith. *U.S. Patent No. 5,186,987*.

Jianghong, X., Yiou, W. and Ding, Y. (2015). A Shear Deformation Theory for Bending and Buckling of Undersea Sandwich Pipes. *Composite Structures*. 132: 633-43.

Karbhari, V.M. (2015). Rehabilitation of pipelines using fiber-reinforced polymer (FRP) composites.

Kim, S. H., Yoon, S. J., & Choi, W. (2019). Experimental Study on Long-Term Ring Deflection of Glass Fiber-Reinforced Polymer Mortar Pipe. *Advances in Materials Science and Engineering*. 2019: #D 6937540.

Kittson, M. and Kulawic, S. (1998). Pressure-expandable conduit liner. *U.S. Patent No. 5,836,357*.

Lebofsky, S. (2013). Numerically Generated Tangent Stiffness Matrices for Geometrically Non-Linear Structures. Master's Thesis. Department of Aeronautics and Astronautics. University of Washington, USA.

Lee, D.C. and Karbhari, V.M. (2005). Rehabilitation of Large Diameter Prestressed Cylinder Concrete Pipe (PCCP) with FRP Composites – Experimental Investigation. *Advances in Structural Engineering*. 8(1):31-44.

Liu, H., Luo, B. and Li, L. (2017). Design and Mechanical Tests of FRP Pipe with Bamboo and Veneer Layer. *BioResources*. 12(2):2699-2710.

Mai, V. T., Hoult, N. A., & Moore, I. D. (2014). Effect of deterioration on the performance of corrugated steel culverts. *Journal of Geotechnical and Geoenvironmental Engineering*. 140(2): 04013007.

McCracken, A. and Sadeghian, P. (2018). Corrugated Cardboard Core Sandwich Beams with Bio Based Flax Fiber Composite Skins. *Journal of Building Engineering*. 20:114-122.

McCracken, A. and Sadeghian, P. (2018). Partial-Composite Behavior of Sandwich Beams Composed of Fiberglass Facesheets and Woven Fabric Core. *Thin-Walled Structures*. 131:805-815.

Parashar, A. and Mertiny, P. (2011). Impact of Scaling on Fracture Strength of Adhesively Bonded Fiber-reinforced Polymer Piping. *Procedia Engineering*. 10: 455-59.

Park, J., Hong, W., Lee, W., Park, J. and Yoon, S. (2014). Pipe Stiffness Prediction of Buried GFRP Flexible Pipe. *Polymers & Polymer Composites*. 22(1):17-23.

Rafiee, R and Habibagahi, M.R. (2018). Evaluating mechanical performance of GFRP pipes subjected to transverse loading. *Thin-Walled Structures*. 131:347-359.

Rafiee, R and Habibagahi, M.R. (2018). On the Stiffness Prediction of GFRP Pipes Subjected to Transverse Loading. *KSCE Journal of Civil Engineering*. 22(11):4564-4572.

Rafiee, R. (2016). On the mechanical performance of glass-fiber-reinforced thermosetting-resin pipes: A review. *Composite Structures*. 143:151–164.

Rafiee, R. and Elasmi, F. (2017). Theoretical modeling of fatigue phenomenon in composites pipes. *Composite Structures*. 161:256-263.

Simpson, B., Hoult, N.A. and Moore, I.D. (2017). Rehabilitated reinforced concrete culvert performance under surface loading. *Tunnelling and Underground Space Technology*. 69:52-63.

Spangler, M.G. (1941). The Structural Design of Flexible Pipe Culverts. Bulletin No. 153, Iowa Engineering Station, Ames, IA.

Syachrani, S., Jeong, H.S., Rai, V., Chae, M.J. and Iseley, T. (2010). A risk management approach to safety assessment of trenchless technologies for culvert rehabilitation. *Tunnelling and Underground Space Technology incorporating Trenchless Technology Research*. 25(6):681-688.

Tarakcioglu, N., Samanci, A., Arikan, H., and Akdemir, A. (2007). The fatigue behavior of (±55°)3 filament wound GRP pipes with a surface crack under internal pressure. *Composite Structures*. 80(2):207-211.

Wakayama, S., Kobayashi, S., Kiuchi, N., Sohda, Y. and Matsumoto, T. (2002). Improvement of the burst strength of FW-FRP composite pipes after impact using low-modulus amorphous carbon fiber. *Advanced Composite Materials*. 11(3):319-330.

Walsh, T. (2017). The Plastic Piping Industry in North America. *Applied Plastics Engineering Handbook (Second Edition)*. 697-716.

Wang, Z., Chen, Z., He, Y. and Liu, H. (2017). Numerical Study on Lateral Buckling of Fully Bonded Sandwich Pipes. *International Journal of Steel Structures*. 17(3):863-875.

Wang, Z., Ma, X., Liu, Y. and Hui, M.A. and Guo, H. (2016). The Mechanical Behavior and Failure Mode of FRP Composite Steel Casing Joints. *Polymers and Polymer Composites*. 24(2): 91-97.

Wyant, D. C. (2002). Assessment and rehabilitation of existing culverts, Vol 303. Transportation Research Board - National Cooperative Highway Research Program (NCHRP).

Zhao, J.Q., Rajani, B.B. and NRC Institute for Research in Construction. (2002). Construction and Rehabilitation Costs for Buried Pipe with a Focus on Trenchless Technologies.

Zinno, A., Fusco, E., Prota, A. and Manfredi, G. (2010). Multiscale approach for the design of composite sandwich structures for train application. *Composite Structures*. 92: 2208–2219.

APPENDIX A MATHCAD CODE OF THE ANALYTICAL MODEL

A.1 INTRODUCTION

Mathcad was used to generate an analytical model that encapsulates the concept of FRP liners exhibiting a geometric non-linear behavior while being loaded under transverse compression. The code for initial two iterations for both solid wall and sandwich liners are presented below. A load of 500 N was subsequently added at the end of every iteration to find the diametrical deflection and strains at springline and crown/invert. At the end of every iteration, the circular liner becomes more elliptical, thereby undergoing large deformations which causes it to behave non-linearly. The verification of model against the test data is discussed in Chapter 4 of this manuscript.

A.2 CODE FOR SOLID WALL LINERS

FIRST ITERATION

Vertical _Deflection

$a = 170.21$ $E = 26871$ $F = 500$ F_in_N

$b = 170.21$ $I = 1978$ Dim_in_mm

$$\rho(\theta) = \frac{a.b}{\sqrt[2]{((b^2 \cdot \cos(\theta)^2) + (a^2 \cdot \sin(\theta)^2))}}$$

$$I_1 = \int_0^{\pi/2} \rho(\theta)^2 \cos(\theta)\, d\theta = 2.897 \,.\, 10^4$$

$$I_2 = \int_0^{\frac{\pi}{2}} \rho(\theta)\, d\theta = 267.365$$

$$I_3 = \int_0^{\frac{\pi}{2}} \left(\rho(\theta) \cdot \cos(\theta) - \frac{I_1}{I_2}\right) . \rho(\theta)^2 \cdot \cos(\theta)\, d\theta = 7.337 .10^5$$

$$\Delta V = I_3 \cdot \frac{F}{E \cdot I} = 6.902$$

Horizontal_Deflection

$$I_4 = \int_0^{\pi/2} \rho(\theta)^2 \sin(\theta)\, d\theta = 2.897 . 10^4$$

$$I_5 = \int_0^{\frac{\pi}{2}} \left(\left(\frac{I_1}{I_2}\right) - \rho(\theta)\cos(\theta)\right)\left(\rho(\theta)\sin(\theta) - \left(\frac{I_4}{I_2}\right)\right) . \rho(\theta)\, d\theta = 6.737 . 10^5$$

$$\Delta H = I_5 \cdot \frac{F}{E \cdot I} = 6.338$$

Calculation_of_new_a_and_b

$$a = a + \frac{\Delta H}{2} = 173.379$$

$$b = b - \frac{\Delta V}{2} = 166.759$$

Calculation_for_M_and_N

$$\Delta F = 500$$

$$M_A = \frac{I_1 \cdot \Delta F}{2 \cdot I_2}$$

$$M(\theta) = M_A - \frac{\Delta F}{2}\rho(\theta)\cos(\theta)$$

$$M(0) = -1.546 .10^4$$

$$M\left(\frac{\pi}{2}\right) = 2.709 .10^4$$

$$\alpha(\theta) = a\tan\left(\frac{-b^2}{a^2}\cdot\frac{1}{\tan(\theta)}\right)\text{rad}$$

$$\Delta N(\theta) = \frac{-\Delta F}{2}.\sin\left(\alpha(\theta)\right)$$

$$N\ (0.0000001) = 250$$

$$N\left(\frac{\pi}{2}\right) = 1.416\cdot 10^{-14}$$

SECOND ITERATION

$$\rho(\theta) = \frac{a.b}{\sqrt[2]{((b^2\cdot\cos(\theta)^2) + (a^2\cdot\sin(\theta)^2))}}$$

$$I_1 = \int_0^{\pi/2} \rho(\theta)^2\cos(\theta)\,d\theta = 2.929\,.10^4$$

$$I_2 = \int_0^{\frac{\pi}{2}} \rho(\theta)\,d\theta = 267.068$$

$$I_3 = \int_0^{\frac{\pi}{2}} \left(\rho(\theta)\cdot\cos(\theta) - \frac{I_1}{I_2}\right).\rho(\theta)^2\cdot\cos(\theta)\,d\theta = 7.635\,.10^5$$

$$\Delta V = I_3\cdot\frac{F}{E\cdot I} = 7.183$$

Horizontal_Deflection

$$I_4 = \int_0^{\pi/2} \rho(\theta)^2\sin(\theta)\,d\theta = 2.854\,.10^4$$

$$I_5 = \int_0^{\frac{\pi}{2}} \left(\left(\frac{I_1}{I_2}\right) - \rho(\theta)\cos(\theta)\right)\left(\rho(\theta)\sin(\theta) - \left(\frac{I_4}{I_2}\right)\right).\rho(\theta)\,d\theta = 6.716\,.10^5$$

$$\Delta H = I_5 \cdot \frac{F}{E \cdot I} = 6.318$$

Calculation_of_new_a_and_b

$$a = a + \frac{\Delta H}{2} = 176.538$$

$$b = b - \frac{\Delta V}{2} = 163.168$$

Calculation_for_M_and_N

$$\Delta F = 500$$

$$M_A = \frac{I_1 \cdot \Delta F}{2 \cdot I_2}$$

$$\Delta M(\theta) = M_A - \frac{\Delta F}{2} \rho(\theta) \cos(\theta)$$

$$\Delta M(0) = -1.593 .10^4$$

$$\Delta M\left(\frac{\pi}{2}\right) = 2.741 .10^4$$

$$M(\theta) = M(\theta) + \Delta M(\theta)$$

$$M(0) = -3.139 . 10^4$$

$$M\left(\frac{\pi}{2}\right) = 5.45 \cdot 10^4$$

$$\alpha(\theta) = a\tan\left(\frac{-b^2}{a^2} \cdot \frac{1}{\tan(\theta)}\right) \text{rad}$$

$$\Delta N(\theta) = \frac{-\Delta F}{2} . \sin\left(\alpha(\theta)\right)$$

$$\Delta N\ (0.0000001) = 250$$

$$\Delta N\left(\frac{\pi}{2}\right) = 1.308 \cdot 10^{-14}$$

$$N(\theta) = N(\theta) + \Delta N(\theta)$$

$N(0.0000001) = 500$

$N\left(\frac{\pi}{2}\right) = 2.724 \cdot 10^{-14}$

A.3 Code for Sandwich Liners

First Iteration

Vertical_and_Horizontal_Deflection

$a = 167.85$ $w = 304.75$ $c = 4.35$ F_in_N

$b = 167.85$ $d = 6.95$ $G = 144$ Dim_ in_mm

$EI = 436532790$

$A = w.\frac{d^2}{c}$

$\alpha(\theta) = a\tan\left(\frac{-b^2}{a^2} \cdot \frac{1}{\tan(\theta)}\right) rad$

$N(\theta, F) = \frac{-F}{2} \cdot \sin(\alpha(\theta))$

$V(\theta, F) = \frac{-F}{2} \cdot \cos(\alpha(\theta))$

$\rho(\theta) = \frac{a.b}{\sqrt[2]{((b^2 \cdot \cos(\theta)^2) + (a^2 \cdot \sin(\theta)^2))}}$

$I_1 = \int_0^{\pi/2} \rho(\theta)^2 \cos(\theta)\, d\theta = 2.817 \,.\, 10^4$

$I_2 = \int_0^{\frac{\pi}{2}} \rho(\theta)\, d\theta = 263.658$

$M_A(F) = \frac{I_1 \cdot F}{2 \cdot I_2}$

$$M(\theta, F) = M_A(F) - \frac{F}{2}\rho(\theta)\cos(\theta)$$

$$U_b(F) = 4 \cdot \int_0^{\pi/2} M(\theta, F)^2 \frac{\rho(\theta)}{2 \cdot EI} d\theta$$

$$U_s(F) = 4 \cdot \int_0^{\pi/2} V(\theta, F)^2 \frac{\rho(\theta)}{2 \cdot GA} d\theta$$

$$U(F) = U_b(F) + U_s(F)$$

$$\delta V(F) = \frac{d}{dF} U(F)$$

$$F = 500$$

$$\delta V(F) = 0.941$$

$$I_3 = \int_0^{\frac{\pi}{2}} \left(\rho(\theta) \cdot \cos(\theta) - \frac{I_1}{I_2}\right) . \rho(\theta)^2 \cdot \cos(\theta)\, d\theta$$

$$I_4 = \int_0^{\pi/2} \rho(\theta)^2 \sin(\theta)\, d\theta$$

$$I_5 = \int_0^{\frac{\pi}{2}} \left(\left(\frac{I_1}{I_2}\right) - \rho(\theta)\cos(\theta)\right)\left(\rho(\theta)\sin(\theta) - \left(\frac{I_4}{I_2}\right)\right) . \rho(\theta)\, d\theta$$

$$M(\theta, F, Q) = \frac{F}{2}\left(\left(\frac{I_1}{I_2}\right) - \rho(\theta)\cos(\theta)\right) + \frac{Q}{2}\left(\rho(\theta)\sin(\theta) - \frac{I_4}{I_2}\right)$$

$$U_b(F, Q) = 4 \cdot \int_0^{\pi/2} M(\theta, F, Q)^2 \frac{\rho(\theta)}{2 \cdot EI} d\theta$$

$$U_s(F) = 4 \cdot \int_0^{\pi/2} V(\theta, F)^2 \frac{\rho(\theta)}{2 \cdot GA} d\theta$$

$$U(F, Q) = U_b(F, Q) + U_s(F)$$

$$\delta H(F, Q) = \frac{d}{dQ} U(F, Q)$$

$F=500$

$Q=0$

$$\delta H(F, Q) = 0.74$$

Calculation_of_new_a_and_b

$$a = a + \frac{(\delta H(500,0))}{2} = 168.22$$

$$b = b - \frac{(\delta V(500))}{2} = 167.379$$

Calculation_for_M_and_N

$$\Delta F = 500$$

$$M_A(\Delta F) = \frac{I_1 \cdot \Delta F}{2 \cdot I_2}$$

$$M_1(\theta, \Delta F) = M_A(\Delta F) - \frac{\Delta F}{2} \rho(\theta) \cos(\theta)$$

$$\theta = 0$$

$$M_1(\theta, \Delta F) = -1.525 \cdot 10^4$$

$$\theta = \frac{\pi}{2}$$

$$M_1(\theta, \Delta F) = 2.671 \cdot 10^4$$

$$\alpha(\theta) = a \tan\left(\frac{-b^2}{a^2} \cdot \frac{1}{\tan(\theta)}\right) \text{rad}$$

$$N_1(\theta, \Delta F) = \frac{-\Delta F}{2} . \sin\left(\alpha(\theta)\right)$$

$$\theta = 0.0000001$$

$$N_1(\theta, \Delta F) = 250$$

$$\theta = \frac{\pi}{2}$$

$$N_1(\theta, \Delta F) = 1.515 \ . 10^{-14}$$

SECOND ITERATION

$$\alpha(\theta) = a\tan\left(\frac{-b^2}{a^2} \cdot \frac{1}{\tan(\theta)}\right) \text{rad}$$

$$N(\theta, F) = \frac{-F}{2} \cdot \sin\left(\alpha(\theta)\right)$$

$$V(\theta, F) = \frac{-F}{2} \cdot \cos\left(\alpha(\theta)\right)$$

$$\rho(\theta) = \frac{a . b}{\sqrt[2]{((b^2 \cdot \cos(\theta)^2) + (a^2 \cdot \sin(\theta)^2))}}$$

$$I_1 = \int_0^{\pi/2} \rho(\theta)^2 \cos(\theta)\, d\theta = 2.82 . 10^4$$

$$I_2 = \int_0^{\frac{\pi}{2}} \rho(\theta)\, d\theta = 263.578$$

$$M_A(F) = \frac{I_1 \cdot F}{2 \cdot I_2}$$

$$M(\theta, F) = M_A(F) - \frac{F}{2}\rho(\theta)\cos(\theta)$$

$$U_b(F) = 4 \cdot \int_0^{\pi/2} M(\theta, F)^2 \frac{\rho(\theta)}{2 \cdot EI} d\theta$$

$$U_s(F) = 4 \cdot \int_0^{\pi/2} V(\theta, F)^2 \frac{\rho(\theta)}{2 \cdot GA} d\theta$$

$$U(F) = U_b(F) + U_s(F)$$

$$\delta V(F) = \frac{d}{dF} U(F)$$

$$F = 500; \quad \delta V(F) = 0.945$$

$$I_3 = \int_0^{\frac{\pi}{2}} \left(\rho(\theta) \cdot \cos(\theta) - \frac{I_1}{I_2}\right) . \rho(\theta)^2 \cdot \cos(\theta)\, d\theta$$

$$I_4 = \int_0^{\pi/2} \rho(\theta)^2 \sin(\theta)\, d\theta$$

$$I_5 = \int_0^{\frac{\pi}{2}} \left(\left(\frac{I_1}{I_2}\right) - \rho(\theta)\cos(\theta)\right)\left(\rho(\theta)\sin(\theta) - \left(\frac{I_4}{I_2}\right)\right) . \rho(\theta)\, d\theta$$

$$M(\theta, F, Q) = \frac{F}{2}\left(\left(\frac{I_1}{I_2}\right) - \rho(\theta)\cos(\theta)\right) + \frac{Q}{2}\left(\rho(\theta)\sin(\theta) - \frac{I_4}{I_2}\right)$$

$$U_b(F, Q) = 4 \cdot \int_0^{\pi/2} M(\theta, F, Q)^2 \frac{\rho(\theta)}{2 \cdot EI} d\theta$$

$$U_s(F) = 4 \cdot \int_0^{\pi/2} V(\theta, F)^2 \frac{\rho(\theta)}{2 \cdot GA} d\theta$$

$$U(F, Q) = U_b(F, Q) + U_s(F)$$

$$\delta H(F, Q) = \frac{d}{dQ} U(F, Q)$$

$Q = 0; \quad \delta H(F, Q) = 0.739$

Calculation_of_new_a_and_b

$$a = a + \frac{\left(\delta H(F, Q)\right)}{2} = 168.59$$

$$b = b - \frac{\left(\delta V(F)\right)}{2} = 166.907$$

Calculation_for_M_and_N

$$M_A(\Delta F) = \frac{I_1 \cdot \Delta F}{2 \cdot I_2}$$

$$\Delta M(\theta, \Delta F) = M_A(\Delta F) - \frac{\Delta F}{2} \rho(\theta) \cos(\theta)$$

$$M_1(\theta, \Delta F) = \Delta M(\theta, \Delta F) + M_1(\theta, \Delta F)$$

$$\theta = 0$$

$$M_1(\theta, \Delta F) = -3.055 \cdot 10^4$$

$$\theta = \frac{\pi}{2}$$

$$M_1(\theta, \Delta F) = 5.346 \cdot 10^4$$

$$\alpha(\theta) = a \tan\left(\frac{-b^2}{a^2} \cdot \frac{1}{\tan(\theta)}\right) \text{rad}$$

$$\Delta N(\theta, \Delta F) = \frac{-\Delta F}{2} . \sin\left(\alpha(\theta)\right)$$

$$N_1(\theta, \Delta F) = \Delta N(\theta, \Delta F) + N_1(\theta, \Delta F)$$

$$\theta = 0.0000001$$

$$N_1(\theta, \Delta F) = 500$$

$$\theta = \frac{\pi}{2}$$

$$N_1(\theta, \Delta F) = 3.016 \cdot 10^{-14}$$

APPENDIX B TENSILE COUPON TEST METHOD AND RESULTS

B.1 INTRODUCTION

The coupon tensile test was conducted by McCracken and Sadeghian (2018) for their study on "Partial-Composite Behavior of Sandwich Beams Composed of Fiberglass Facesheets and Woven Fabric Core" using the same materials used for this research. The test conformed with ASTM D3039, which is the standard test method for determining the tensile properties of polymer matrix composite materials reinforced with high modulus fibers. Although, only composites with continuous fiber or discontinuous fiber-reinforced composites in which the laminates are balanced and symmetric with respect to the test direction can be tested (ASTM 2017).

B.2 SPECIMEN FABRICATION

1. According to ASTM D3039 standards, five identical tensile coupons were made using two layers of unidirectional fabrics (either glass or carbon) and epoxy resin by wet lay-up method.
2. As the standards suggest, the coupons were fabricated with two tabs attached to the ends of each side of the coupon. The size of the coupon was 25 x 250 mm and the size of each tab was 25 x 62.5 mm.
3. The tabs were used to aid the coupons in gripping while being tested. It ensured that the gripping did not produce any stress concentrations or premature failures. Figure 1 shows the dimension parameters of the coupon.

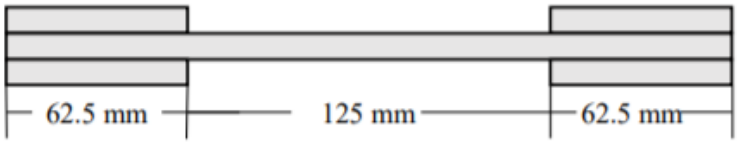

Figure 1 Dimension Details of Coupon (McCracken and Sadeghian 2018)

4. At the mid-height of the length of each coupon, a strain gauge was applied on each side in alignment with the fiber direction to measure its axial strain.

B.3 Results of Coupon Testing

The coupons were tested under a UTM with a capacity of 100 kN with a displacement rate of 2 mm/min. The results of tensile test found based on a ply thickness of 1.3 mm (glass) and 1.24 mm (carbon) are reported in Figure 2. The ply thicknesses are as reported by the manufacturer. The GFRP coupons had an average tensile strength of 583 ± 31 MPa and an average elastic modulus of 21.75 ± 0.58 GPa. Similarly, CFRP had an average tensile strength of 1126 MPa and an elastic modulus of 100 GPa. Figure 2 shows the linear behavior displayed by the coupons up to the point of rupture.

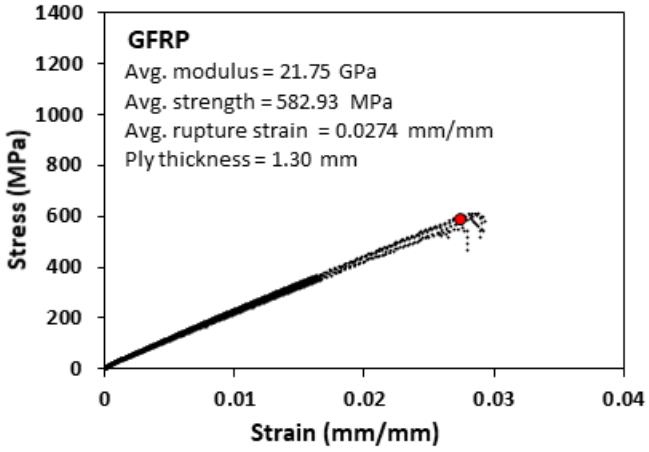

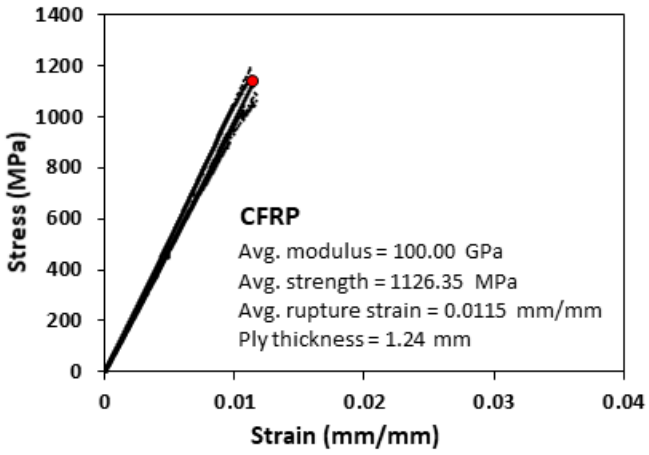

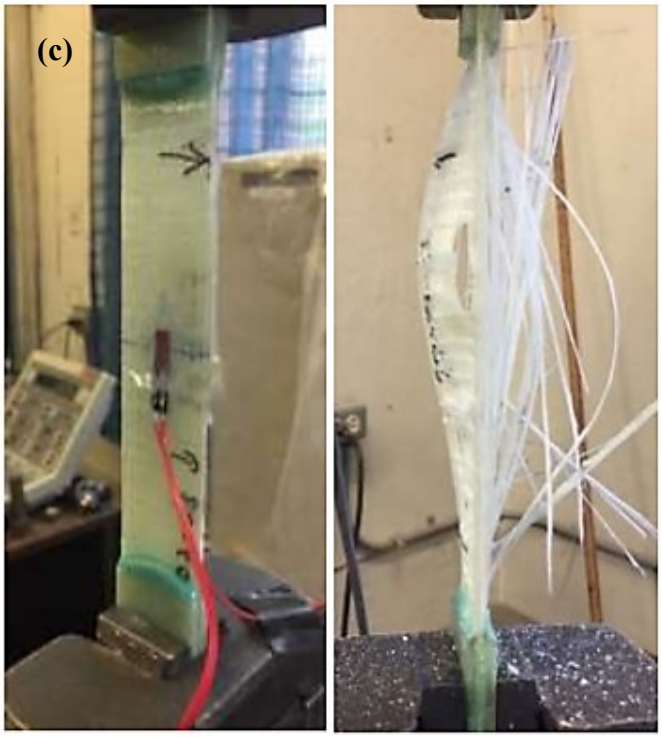

Figure 2 Testing FRP in Tension: Stress-Strain Curves for (a) GFRP (b) CFRP; (c) Coupon Before and After Testing (McCracken and Sadeghian 2018)

B.4 FORMULAS USED

1. Ultimate Tensile Strength

   The ultimate tensile strength is calculated as:

$$F^{tu} = \frac{P^{max}}{A} \quad (1)$$

   where,

   F^{tu} = Ultimate Tensile Strength, MPa

   P^{max} = Maximum Force before Failure, N

   A = Average Cross-Sectional Area, mm^2

2. Ultimate Tensile Strain

$$\varepsilon_i = \frac{\delta_i}{L_g} \tag{2}$$

where,

ε_i = Tensile Strain at i^{th} Data Point, με

δ_i = Extensometer Displacement at i^{th} Data Point, mm

L_g = Extensometer Gage Length, mm

3. Tensile Elastic Modulus

$$E = \frac{\sigma}{\varepsilon} \tag{3}$$

where,

E = Tensile Elastic Modulus, GPa

σ = Ultimate Tensile Strength, MPa

ε = Ultimate Tensile Strain, mm/mm

APPENDIX C RESULTS OF A LASER SCANNING TEST

C.1 INTRODUCTION

A laser scanning test was conducted on the 2G-B-2G and 2C-B-2C specimens by Farzaneh Hamedi Azad (Ph.D. Student, Department of Civil and Resource Engineering, Dalhousie University and Dr. Navid Bahrani (Assistant Professor, Department of Civil and Resource Engineering) using a VERSA3D laser scanner by Clickmox Solutions. This test was conducted to study the deformation shape and to find the deflection which is helpful in determining the ring stiffness of the deformed pipe.

C.2 TEST PROCEDURE

1. A reflective tape was adhered to the springline and crown/invert positions of the liner such that it is sensor receptive.
2. The scanner was placed and centered approximately 600 mm away from the loaded liner. As the scanner emitted laser beams, it rotated about its vertical axis.
3. A scan was done once before the test and once after to capture the actual shape and deformed shape, respectively.
4. The scan time was roughly about 1.5 to 2 minutes, where the scanner captures various targets located around the liner.

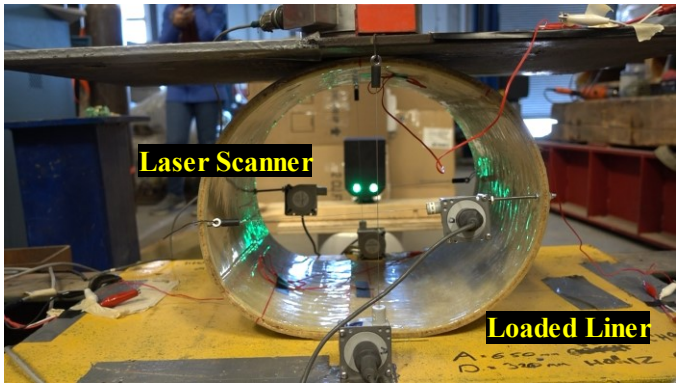

Figure 1 Laser Scanner Capturing the Liner Deformation

C.3 DATA PROCESSING

The data is processed to clear the noises and the liner geometry is edited efficiently in order to measure the deflection levels. The output file is fed into AutoCAD to validate the results obtained from the laser scanning against the experimental test data. It was found that the laser scanning was efficient in determining the liner diameter and the deflections. The results are tabulated in Table 1. AutoCAD output of the calculated measurements are presented in Figure 2.

Table 1 Laser Scanning Result vs. Experimental Results

	Laser Scanning	Experimental Data
Internal Liner Diameter (mm)	328.60	328.39
Vertical Deflection (mm)	154.54	153.71

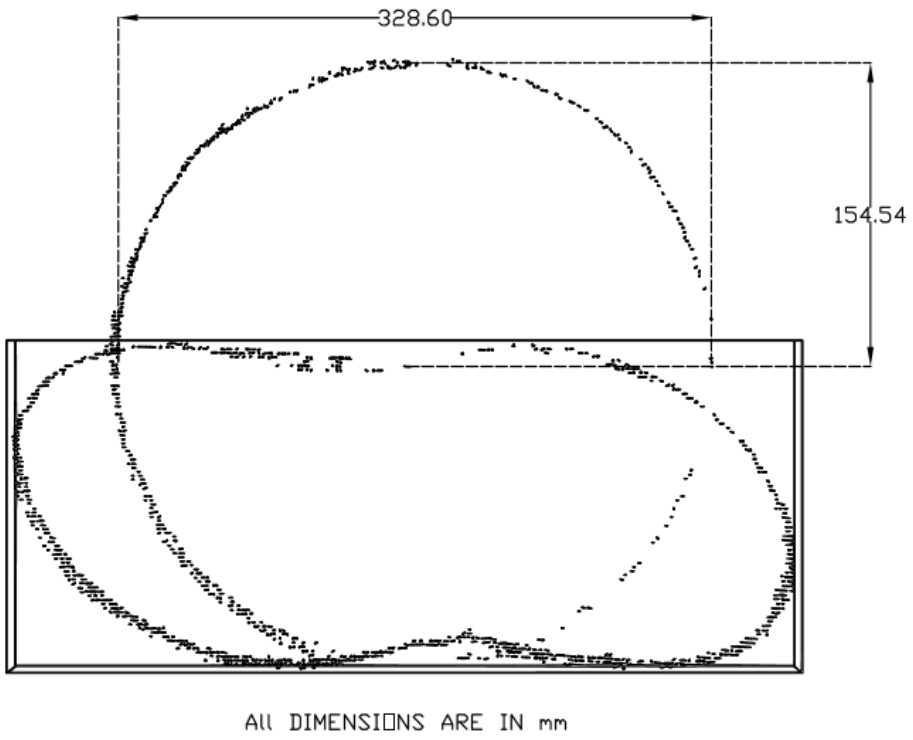

Figure 2 AutoCAD Output of the Calculated Measurements

C.3 LINER DEFORMATION

The failures mode and deformation shape for 2G-B-2G specimen were captured while the test was ongoing. For the 2C-B-2C specimen, only two scans before and after the experimental test, respectively were done.

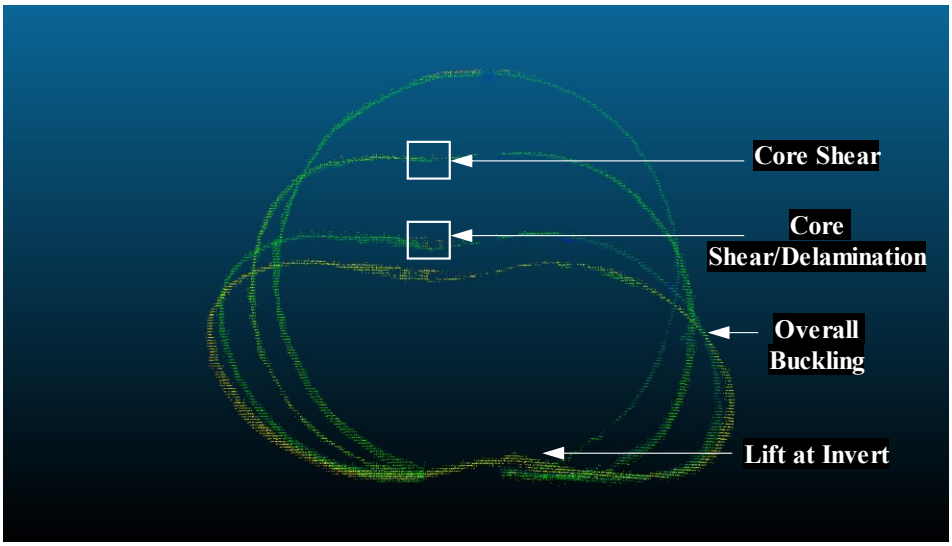

Figure 3 Failure mode and Ultimate Deformation Shape of 2G-B-2G Specimen (Farzaneh and Dr. Bahrani, Dalhousie University)

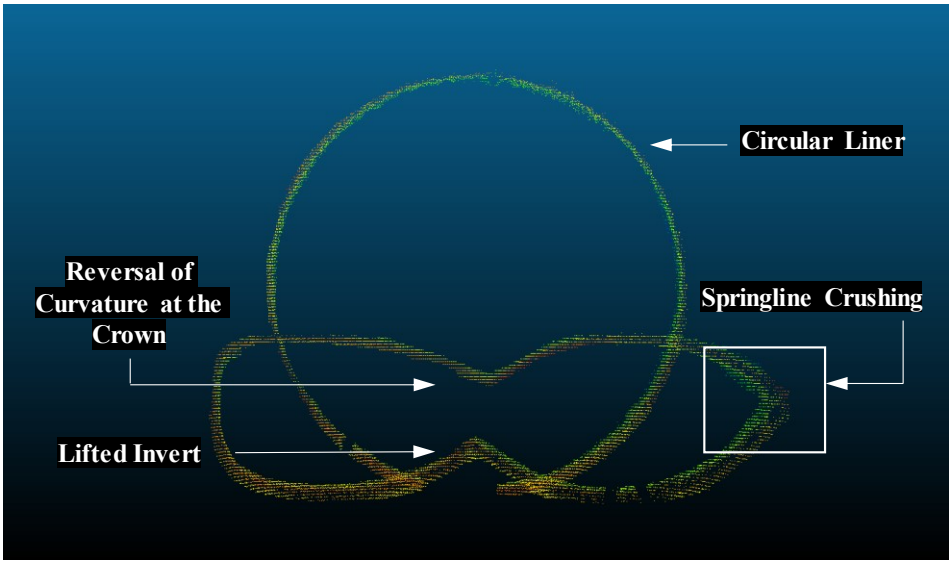

Figure 3 Ultimate Deformation Shape of 2C-B-2C Specimen (Farzaneh and Dr. Bahrani, Dalhousie University)

C.4 CONCLUSION

Based on the laser scanning test, the following can be concluded:

1. The results from laser scanning method are in a very good agreement with the test data. This method of measuring deflections for real time applications or large scale tests would be beneficial in terms of cost and time provided skilled labor is available.
2. For liners/ buried pipes with an uncommon shape geometry such as a pipe arch and underpass, determination of deflection levels and deformation shape is difficult. Using a laser scanners could help understand and determine various geometrical parameters based on their cross-sectional shape.
3. Geometric estimation and location of pipe failures, disruption in hydraulic flow, wall thinning at mid sections of a pipe/liner in service could be easily determined using this test without much human interference.